

*This document has been digitized by the Oil Sands Research and Information Network, University of Alberta with permission of Alberta Environment.*

AN ASSESSMENT OF THE MODELS  
LIRAQ AND ADPIC FOR APPLICATION  
TO THE ALBERTA OIL SANDS AREA

by

D. REID, L. WALMSLEY  
B. FINDLETON, and D. CHRISTIE  
Atmospheric Environment Service  
Downsview, Ontario

for

ALBERTA OIL SANDS ENVIRONMENTAL RESEARCH PROGRAM

Project AS 4.2.3

May 1979

TABLE OF CONTENTS

	Page
DECLARATION. . . . .	ii
LETTER OF TRANSMITTAL. . . . .	iii
DESCRIPTIVE SUMMARY. . . . .	iv
LIST OF TABLES . . . . .	xi
LIST OF FIGURES. . . . .	xii
ABSTRACT . . . . .	xiii
ACKNOWLEDGEMENTS . . . . .	xiv
1. INTRODUCTION . . . . .	1
2. CONDITIONS AT THE AOSERP STUDY AREA. . . . .	3
2.1 The AOSERP Study Area. . . . .	3
2.2 Emissions. . . . .	6
2.3 Meteorological Conditions of Concern . . . . .	10
2.4 Plume Pollutant Chemistry. . . . .	13
2.5 Deposition to the Surface. . . . .	14
3. THE ADPIC MODEL. . . . .	16
3.1 Introduction to ADPIC. . . . .	16
3.2 MATHEW . . . . .	16
3.2.1 Aspects of the Calculus of Variations . . . . .	17
3.2.2 The Variational Method Applied to MATHEW. . . . .	19
3.2.3 Boundary Conditions . . . . .	21
3.2.4 Numerical Techniques. . . . .	21
3.2.5 Selection of Model Parameters . . . . .	22
3.2.6 Derivation of the Observed Wind Field . . . . .	23
3.2.7 Data Requirements . . . . .	24
3.2.8 Computer Requirements . . . . .	26
3.2.9 Application and Verification. . . . .	27
3.2.10 Evaluation. . . . .	28
3.3 ADPIC. . . . .	30
3.3.1 Eulerian-Lagrangian Particle-in-Cell Method. . . . .	32
3.3.2 Boundary Conditions . . . . .	33
3.3.3 Numerical Techniques . . . . .	34
3.3.4 Data Requirements . . . . .	36
3.3.5 Computer Requirements . . . . .	37
3.3.6 Application and Verification. . . . .	37
3.3.7 Evaluation. . . . .	39
3.4 PATRIC . . . . .	39

TABLE OF CONTENTS (CONCLUDED)

	Page
4. THE LIRAQ MODEL. . . . .	42
4.1 Introduction to LIRAQ. . . . .	42
4.2 MASCON . . . . .	46
4.2.1 Physical Basis. . . . .	48
4.2.2 Mathematical Basis. . . . .	50
4.2.3 Boundary Conditions and Constraints . . . . .	51
4.2.4 Computational Formulation . . . . .	51
4.2.5 Data Requirements . . . . .	54
4.2.6 Computer Requirements . . . . .	57
4.2.7 Evaluation. . . . .	58
4.3 LIRAQ-1. . . . .	58
4.3.1 Physical Basis. . . . .	60
4.3.2 Eddy Diffusivities. . . . .	65
4.3.3 Boundary Conditions . . . . .	66
4.3.4 Computational Formulation . . . . .	67
4.3.5 Data Requirements . . . . .	68
4.3.6 Computer Requirements . . . . .	69
4.3.7 Evaluation. . . . .	69
4.4 LIRAQ-2. . . . .	69
4.4.1 Model Chemistry . . . . .	71
4.4.2 Computational Formulation . . . . .	75
4.4.3 Data Requirements . . . . .	79
4.4.4 Computer Requirements . . . . .	80
4.4.5 Evaluation. . . . .	80
5. CONCLUSION. . . . .	82
6. RECOMMENDATIONS . . . . .	84
7. REFERENCES CITED . . . . .	85
8. APPENDICES. . . . .	88
8.1 Comparative Computer Resources at LLL and CMC	88
8.2 Chemical Kinetic Concepts . . . . .	89
9. LIST OF AOSERP RESEARCH REPORTS . . . . .	92

LIST OF TABLES

	Page
1. Summary of Emissions . . . . .	7
2. Great Canadian Oil Sands Major Emission Point parameters . . . . .	8
3. Syncrude Major Emission Point Parameters . . . . .	9
4. SO <sub>2</sub> Incidents Monitored at AOSERP Stations, June to December 1977. . . . .	11
5. Diurnal Variation of SO <sub>2</sub> Concentrations Monitored at AOSERP Stations, June to December 1977. .	12
6. Advantages and Disadvantages of MATHEW . . . . .	29
7. Advantages and Disadvantages of ADPIC. . . . .	40
8. Advantages and Disadvantages of MASCON . . . . .	59
9. Advantages and Disadvantages of LIRAQ-1. . . . .	70
10. Reaction Set Used In LIRAQ-2 . . . . .	72
11. Reaction Set Used in LIRAQ-2S. . . . .	76
12. Advantages and Disadvantages of LIRAQ-2. . . . .	81

LIST OF FIGURES

	Page
1. Location of the AOSERP Study Area . . . . .	4
2. Topography of the AOSERP Study Area and Surroundings. .	5
3. Basic Information Flow for LIRAQ . . . . .	44
4. Basic Information Flow for MASCON . . . . .	47
5. Staggered Finite Difference Grid for the MASCON Relaxation . . . . .	52

ABSTRACT

Following previous tentative identification of the computer program packages LIRAQ and ADPIC as useful for application in studying air quality processes in the region of the Athabasca Oil Sands, this report examines these models in greater detail. After a brief examination of the relevant conditions in the area to identify possible (or necessary) simplifications each model is examined in detail. For the LIRAQ program package it is concluded that the model assumptions are too restrictive for application to this problem. The ADPIC program package is found to be more applicable although reactive pollution photochemistry is not handled. The relatively low computer capacity currently available in Canada makes application of this model computationally impractical. A modified version of the ADPIC code, acronym PATRIC, is identified as having potential for AOSERP although the code would need to be almost completely restructured to overcome current physical and computer limitations.

ACKNOWLEDGEMENTS

We wish to acknowledge the co-operation of Lawrence Livermore Laboratory staff M. Dickerson, C. Sherman, R. Lange, W. Duewer, M. MacCracken and group director J. Knox. Their willingness to openly discuss their models during a visit two of the authors made to Lawrence Livermore Laboratory (LLL), California greatly enhanced this evaluation.

We also wish to acknowledge the help of M. Strosher, Alberta Environment, in providing data on deteriorated air quality situations in the oil sands area, and L. Barrie, Atmospheric Environment Service, for assistance with respect to plume oxidation and deposition studies in the area.

The text benefitted substantially from careful reviews by A. Mann of AOSERP and D. Davison in INTERA Environmental Consultants.

This manuscript was capably typed by S. Robinson.

This research project AS 4.3.2 was funded by the Alberta Oil Sands Environmental Research Program, a joint Alberta-Canada research program established to fund, direct, and co-ordinate environmental research in the Athabasca Oil Sands area of north-eastern Alberta.

## 1. INTRODUCTION

Since one of the predominant pathways by which industrial process effluents impact on terrestrial ecosystems is via the atmosphere, the Alberta Oil Sands Environmental Research Program (AOSERP) has pursued the understanding of this pathway as a major program goal. To meet this broad objective, and in addition to extensive field studies, a sequence of modelling approaches has been established. The first approach, Walmsley and Bagg (1977), involved the application of the relatively simple Climatological Dispersion Model to yield average annual ground-level concentrations of sulphur dioxide, and derived dry deposition to the surface, in the immediate development area. A second approach, now underway, is implementing a more complex Gaussian model (acronym CRSTER) with the intention of identifying worst case pollution situations and potentially providing monthly mean concentrations for a larger area of concern. The final approach proposed was for the implementation of more sophisticated models that can incorporate the effects of topography and variable meteorological and chemical processes. Padro (1977) identified two such models, LIRAQ and ADPIC, as having potential to address these concerns.

The objective of this study is to further assess the merits of these two models for solution of medium range impact assessment problems in the AOSERP area. The stage is set for this assessment in Section 2 by reviewing the current knowledge of emissions, critical meteorological conditions, pollutant plume chemistry, and processes of deposition to the surface as they have been defined for the AOSERP area by previous studies. This helps bring into focus the special conditions of the area which these models must be able to simulate to be satisfactory for implementation. The following two sections detail the ADPIC and LIRAQ models, respectively. In reading these discussions it is important to appreciate that, whereas LIRAQ is a well developed package which has been used for practical air quality assessment, ADPIC is still in a developmental stage. A discussion of the extent to which the inherent model assumptions are in accord with the special conditions identified is followed by

assessments of the data requirements, computer implementation, and run time requirements. With respect to computer requirements the assessment relates to the operation of the models on the CDC 7600 computer at the Canadian Meteorological Centre (CMC), the most powerful computer available in Canada for such purposes at the time of writing. Finally the conclusions of the study are presented and recommendations for further action stated.

## 2. CONDITIONS AT THE AOSERP STUDY AREA

Even relatively complex air pollution models, such as LIRAW and ADPIC, are relatively crude representations of the processes actually occurring in the atmosphere. There are three main reasons for this:

1. In most cases our understanding of the physical processes acting is not complete;
2. Computer execution speeds have not yet increased to match the complexity of the problem. The processes to be represented must be limited to the most important, and then usually in rather simplified form; and
3. Available computers have limited storage. Consequently to represent a large area only a relatively few points can be selected.

These limitations dictate that at present air pollution models must be formulated carefully to optimize the representation of physical processes and storage requirements. Models are virtually tailor-made for an area and situation under study, particularly for models incorporating chemical reactions like LIRAQ. It is important then to understand the conditions of the AOSERP area so as to identify simplifications which may be applicable. These are established, as current knowledge permits, in this chapter. A discussion of the conditions under which air quality is likely to be most deteriorated is included as it is only for such episode situations that application of complex models is likely to be cost effective.

### 2.1 THE AOSERP STUDY AREA

From a large scale perspective the area of concern is within a region sloping down from the heights of the Rocky Mountains along the British Columbia-Alberta border toward the southwest and the plains of the southern Mackenzie district of the Northwest Territories. Figure 1 shows this overall context while Figure 2 shows the topography of the immediate AOSERP region. The heights of

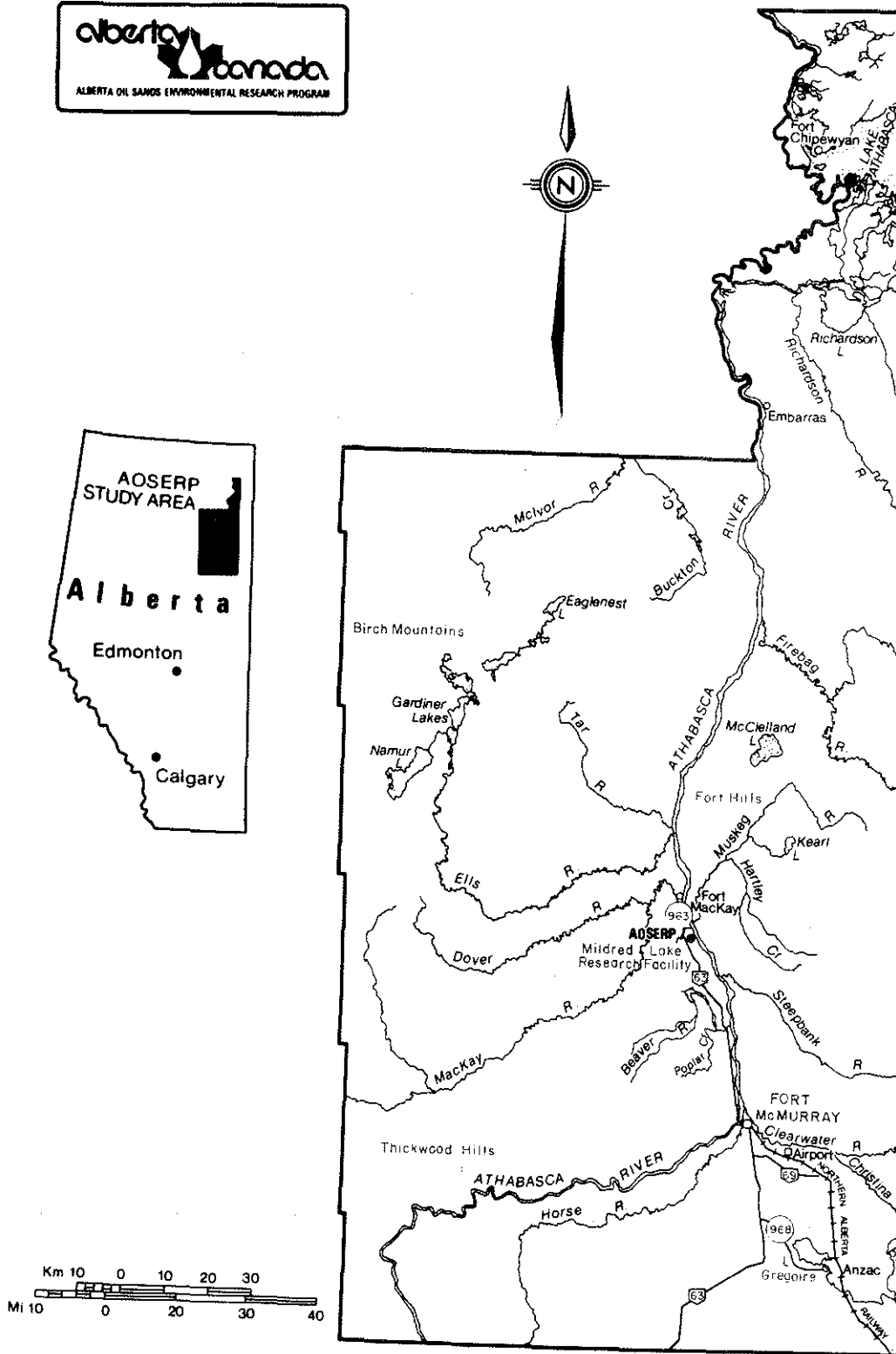


Figure 1. Location of the AOSERP study area.

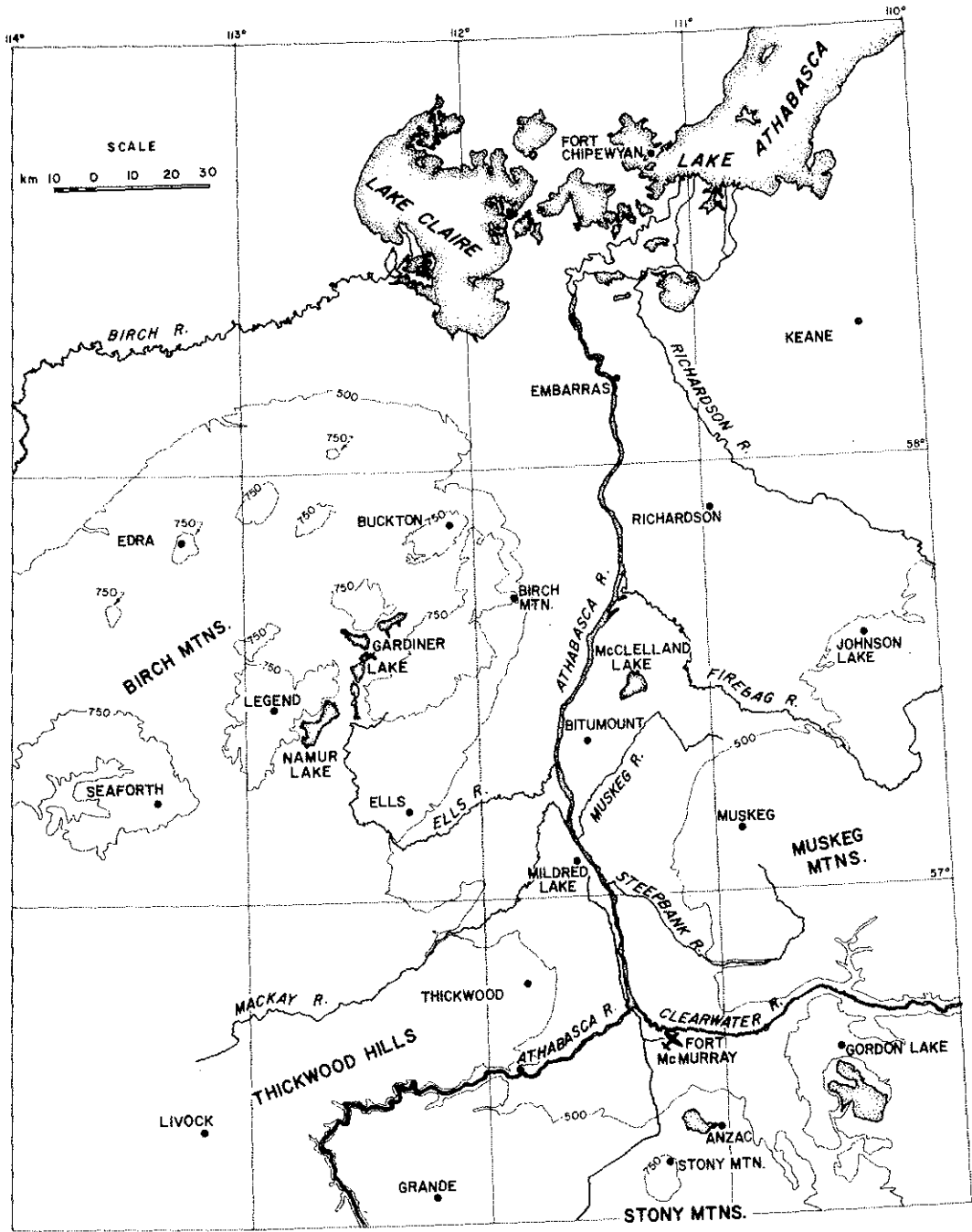


Figure 2. Topography of the AOSERP study area and surroundings.

land are the Birch Mountains, Thickwood Hills, Stony Mountain and Muskeg Mountain. Heights rise to above 800 m in the Birch Mountains. This high ground is cut by numerous rivers, notably the Athabasca and Clearwater rivers running in canyons up to 200 m deep which join north of Fort McMurray. As the Athabasca runs north from Fort McMurray it cuts a progressively less deep canyon, typically 100 m deep in the vicinity of the Great Canadian Oil Sands (GCOS) plant. These steep-sided canyons can be expected to exhibit weak and shallow slope flows running normal to the local topographic contours, and also provide basins for pooling of cold air. Downstream of the present oil recovery plants, the valley broadens and flows into a delta region between Lake Claire and Lake Athabasca (213 m). These broader scale valley features can be expected to provide channelling of prevailing flows and induce valley circulations due to differential diabatic heating for weak overall flow cases. Diabatic valley breezes blow parallel to the large-scale topographic contours and are typically much deeper than the slope flows mentioned previously.

## 2.2 EMISSIONS

A study by Shelfentook (1978) evaluated the emissions in the AOSERP area. Their summary of emissions for 1976 (the latest year available) is reproduced as Table 1. It is clear that for the various pollutants the dominant sources vary.

For sulphur dioxide 1976 emissions were dominated by those from the GCOS plant. With full activation of Syncrude operations  $\text{SO}_2$  emissions will about double to near  $2 \times 10^{11} \text{ g} \cdot \text{yr}^{-1}$ . Tables 2 and 3 (after Strosher 1978) show the break-down of these  $\text{SO}_2$  emissions by source, along with the stack parameters for GCOS and Syncrude, respectively. For any pollutant, such as  $\text{SO}_2$ , where the emissions are dominated by large point sources, due account needs to be taken of plume rise in the simulation. The location of the GCOS plant, within the immediate river trench and with stack heights at a level comparable to that of the surrounding terrain, suggests

Table 1. Summary of emissions.

SOURCE OWNERSHIP	SO <sub>2</sub>	H <sub>2</sub> S	CO	LIGHT HC (AS CH <sub>4</sub> )	RCHO (AS HCHO)	HEAVY ORGANICS	ORGANIC ACIDS	NH <sub>3</sub>	NO <sub>x</sub> (AS NO <sub>2</sub> )	PARTI- CULATES	WATER VAPOR
	10 <sup>6</sup> g	10 <sup>6</sup> g	10 <sup>6</sup> g	10 <sup>6</sup> g	10 <sup>6</sup> g	10 <sup>6</sup> g	10 <sup>6</sup> g	10 <sup>6</sup> g	10 <sup>6</sup> g	10 <sup>6</sup> g	10 <sup>9</sup> g
1.											
NATURAL SOURCES											
a) Forests	1.09	11833.3	289.29	50058.8		184072.		184072.	124915.7	81.8	8406675.0
b) Surface Water											41519.
Sub-Total	1.09	11833.3	289.29	50058.8		184072.		184072.	124915.7	81.8	8448194.0
2.											
MOBILE SOURCES											
a) Roads and Highways	28.5		1272.47	168.7	2.93		2.93		519.1	14313.8	15.4
b) Aircraft	1.0		175.38	10.5					7.8	0.7	1.3
c) Railway	1.0		1.19	2.8	0.08		0.16		6.4	0.5	0.2
d) River Tugs	2.4		1.91	1.4	0.17				2.3	3.3	0.2
Sub-Total	32.9		1450.95	183.4	3.18		3.09		535.6	14317.8	17.1
3.											
TOWNS AND SETTLEMENTS											
a) Fort McMurray	35.1	23.0	1142.17	127.1	7.26	770.0	0.57	357.	1125.6	5113.1	16645.73
b) Fort McKay	0.8		0.52		0.07	0.5			2.2	5.8	0.4
c) Anzac	0.60		0.39		0.05	0.3			1.7	4.3	0.3
Sub-Total	36.5	23.0	1143.08	127.1	7.38	770.8	0.57	357.	1129.5	5123.2	16646.43
4.											
GREAT CANADIAN OIL SANDS	93036.06	13.0	1053.46	326.06	21.78	4633.33	0.12	203.	7368.41	15491.89	13252.68
5.											
SYNCRUDE CANADA	44.47	84.2	632.67	418.20	11.20	1309.00	0.18	1309.	1632.01	34.23	60787.19
6.											
IN SITU											
a) Amoco	110.00		9.30	5.71					159.87	44.35	24.27
b) Texaco	0.11		3.04	0.54					21.64	3.27	18.82
c) Petro-Canada	nil		nil	nil							
Sub-Total	110.11		12.34	6.25					181.51	47.62	43.09
GRAND TOTAL	93261.13	11953.5	4581.79	51119.81	43.54	190785.13	3.96	185941.	135762.73	36096.54	8538923.4

Table 2. Great Canadian Oil Sands major emission point parameters.

Ground Level Elevation: 800 feet (244 m) above sea level.

Definition of Plant North: 32.5° W of true north.

Definition of Plant Reference Point: N 3580' E 4050'

Location of Plant Reference Point: NE corner of LSD 8-23-92-10-W4

	Main Flare	Acid Gas Flare	Powerhouse Stack	Incinerator Stack
Location within plant	N 6175' and E 7185'	N 5963' and E 7185'	N 5297' and E 6155'	N 6061' and E 6509'
Ground level elevation (MSL)	800' (244 m)	800' (244 m)	848' (255 m)	848' (255 m)
Height	325' (99 m)	250' (76.2 m)	350' (106.7 m)	350' (106.7 m)
Tip diameter	3.5' (1.1 m)	1.7' (.52 m)	19' (5.8 m)	5.9' (1.8 m)
Exit temperature	a	a	450°F (232°C)	1000°F (538°C)
SO <sub>2</sub> Emission Rate (g/yr)	0.32x10 <sup>10</sup>	0.85x10 <sup>10</sup>	8.21x10 <sup>10</sup>	0.85x10 <sup>10</sup>

<sup>a</sup> Sulphur emission, flow rate and net BTU values must be obtained for each flaring episode.

Table 3. Syncrude major emission point parameters.

Ground Level Elevation: 1000 feet (305 m) above sea level.

Definition of Plant North: 17°21'15"W of true north.

Definition of Plant Reference Point: 5000' E 0000'N for Drawing No. 50 R-A-1, Rev. 8.

Location of Plant Reference Point: Approximately at the NE corner of LSD 7-1-93-11-W4  
for Drawing No. 50 R-A-1, Rev. 8.

	Main Stack	H <sub>2</sub> S Flare (19F-2)	HC Flare (19F-1)	HC Flare (19F-4)
Location within plant	N 0855' and E 5425'	N 1290' and E 2835'	N 2285' and E 2750'	N 2585' and E 2750'
Ground level elevation (MSL)	1000' (305 m)	980' (299 m)	980' (299 m)	980' (299 m)
Height	600' (183 m)	235' (71.6 m)	250' (76.2 m)	250' (76.2 m)
Tip diameter	26' (7.9 m)	42" (1.06 m)	30" (.76 m)	48" (1.2 m)
Exit temperature	450°F (232°C)	<sup>a</sup>	<sup>a</sup>	<sup>a</sup>
SO <sub>2</sub> Emission Rate (g/yr)	10.4x10 <sup>10</sup>			

<sup>a</sup> Sulphur emission, flow rate and net BTU values must be obtained for each flaring episode.

its emissions are within, or at least close to, a region of substantial non-uniformity of atmospheric flows. Thus, accurate knowledge of the physical emission parameters is important.

Table 1 shows that natural sources dominate the emissions of several chemicals such as hydrogen sulphide, organics, ammonia, oxides of nitrogen, and water vapour. As emphasized by Bottenheim and Strausz (1977), these natural emissions can lead to complex processes of atmospheric chemistry by themselves, and also in combination with anthropogenic emissions.

### 2.3 METEOROLOGICAL CONDITIONS OF CONCERN

In order to better define meteorological conditions of concern for air pollution episodes in the AOSERP study area, and so hopefully identify the model simplifications which may be appropriate,  $\text{SO}_2$  data for the three AOSERP air pollution monitoring stations have been investigated. These stations were selected because they better indicate effects on the scale of interest than the GCOS or Syncrude stations. Table 4 lists the five highest  $\text{SO}_2$  concentration occurrences during the period of record available, June to December 1977, for which no unusual emissions were occurring. Because of the short period of record, and also limited resources available for the analysis, the conclusions here must be regarded as quite tentative.

Table 4 shows the highest recorded 0.5 hour average  $\text{SO}_2$  concentration of 0.14 ppm was at the Bitumount Tower site on 12 June. To put this value in perspective, the Alberta provincial half hour  $\text{SO}_2$  objective is 0.20 ppm, well above the maximum concentration observed. Synoptically the pollution incidents at Bitumount tend to be identified with low pressure troughs over Alberta and with high pressure to the east. The geostrophic flow is consistent with pollution parcel trajectories from the oil sands plants to the Bitumount Tower. Table 5 shows the mean  $\text{SO}_2$  concentration for each hour at Bitumount. There is no diurnal variation apparent. Perhaps the presence of cloud indicated for the incident situations dampens diurnal flow effects.

Table 4. SO<sub>2</sub> Incidents Monitored at AOSERP stations, June to December 1977.

Station	Date mo/day	Max 1/2 hr SO <sub>2</sub> ppm	Time of Max MST	Duration of Readings 0.1 ppm
Bitumount	6/7	0.08	8:00	7:00- 8:30
Tower	6/12	0.13	9:00	7:00-12:30
	10/23	0.07	11:00	4:00-16:30
	10/29	0.06	11:00	9:30-13:00
	12/16	0.05	14:30	12:30-17:00
Fort	8/20	0.07	14:00	10:30-17:30
McMurray	8/30	0.04	2:00	8/29/20:30-8/30/5:00
	11/16	0.10	17:30	14:00-24:30
	7/7	0.04	11:00	9:00-13:00
	9/14	0.04	11:00	9:30-13:00
Birch	7/4	0.02	17:30-24:30	7/3/1:00-7/4/24:30
Mtn.	7/29	0.05	6:00	5:00-8:00
	9/17	0.05	2:00	1:30-7:30
	9/20	0.02	19:30	19:00-24:30
	10/8	0.07	9:00	6:00-11:30

Table 5. Diurnal variation of SO<sub>2</sub> concentrations monitored at AOSERP stations, June to December 1977.

TIME (MST)	AVERAGE HOURLY CONCENTRATIONS (PPM)		
	BITUMOUNT	FORT MCMURRAY	BIRCH MOUNTAIN
1	0.001	0.001	0.000
2	0.000	0.001	0.000
3	0.000	0.001	0.000
4	0.000	0.000	0.000
5	0.000	0.001	0.001
6	0.000	0.001	0.001
7	0.001	0.000	0.001
8	0.000	0.001	0.001
9	0.001	0.001	0.001
10	0.001	0.001	0.001
11	0.001	0.001	0.001
12	0.001	0.001	0.001
13	0.001	0.001	0.001
14	0.001	0.002	0.001
15	0.001	0.002	0.001
16	0.001	0.002	0.000
17	0.000	0.002	0.001
18	0.000	0.002	0.001
19	0.000	0.002	0.001
20	0.001	0.001	0.001
21	0.000	0.001	0.001
22	0.000	0.001	0.001
23	0.000	0.001	0.001
24	0.001	0.001	0.001

The pollution incident data for the Fort McMurray station show lower concentration than for Bitumont. Synoptically favoured situations are lower pressure to the east with geostrophic flow from the north, and frequently a high pressure ridge close to the oil sands area. This would in all likelihood be an inversion limited mixing condition. The diurnal variability (Table 5) is quite marked with an afternoon concentration maximum indicating enhancement of the synoptic flow by up-valley diabatically induced breezes under these clear sky situations.

Data for the Birch Mountain station indicate a maximum observed a 0.5 hour  $\text{SO}_2$  concentration of 0.07 ppm. These low values appear to be associated with low pressure troughs or low pressure centers in Alberta. It appears that the pollutant trajectories to Birch Mountain could often be rather tortuous. Table 5 shows that there is no consistent diurnal trend for Birch Mountain  $\text{SO}_2$  pollution. It should be noted that recent studies at this site have indicated the possibility of contamination from two local diesel power generators.

These preliminary analyses show that pollution incidents at the AOSERP stations most directly affected tend to occur with synoptic trajectories directly from the oil sands plants to the monitoring sites. At least under some circumstances it appears that limited mixing conditions are occurring and diurnal diabatic flow supplements the synoptic flow. Thus a variety of synoptic situations may be important for elevated AOSERP ground level concentrations. Adoption of a model suitable for only a single type situation, limited mixing for example, would not appear to be appropriate now. Further post-mortem type studies are needed to define these conditions more clearly.

#### 2.4 PLUME POLLUTANT CHEMISTRY

Bottenheim and Strausz (1977) give a comprehensive review of the atmospheric chemistry to be expected in the AOSERP area. They stress the problems of transferring knowledge about the chemical processes occurring from other climatic regions, and find little in

the literature with respect to the oil sands latitudes. The important influences are the wide range of ambient temperatures and incident solar radiation.

Some field evidence with respect to these influences has been presented by Lusia et al. (1978) who studied the GCOS plume using a helicopter. They observed a systematic variation in  $\text{SO}_2$  oxidation rate. During the winter studies, and for low solar elevation during the summer,  $\text{SO}_2$  oxidation was undetectable (a rate less than  $0.5\% \cdot \text{h}^{-1}$ ). The presence of several potentially catalytic metals in the plume does not appear to be causing important heterogeneous  $\text{SO}_2$  oxidation. Summer month daytime studies show elevated  $\text{SO}_2$  oxidation rates of  $1-3\% \cdot \text{h}^{-1}$ . Homogenous gas-phase reactions involving  $\text{SO}_2$  and various free radical species resulting from photochemical reactions between power plant  $\text{NO}_x$  emissions and residual hydrocarbon emissions are indicated. Additional evidence of photochemical activity was the presence of an ozone bulge downwind in the plume during a number of the summer daytime flights.

## 2.5 DEPOSITION TO THE SURFACE

Extensive observations of dry deposition have been made as part of AOSERP. For sulphur dioxide Barrie and Walmsley (1978) quote deposition velocities (flux to the surface divided by ambient concentration) to snow of  $0.25 \pm 0.20 \text{ cm} \cdot \text{s}^{-1}$ , in reasonable agreement with previous results over snow. This is for a long term average. The deposition velocity variation with atmospheric stability and surface type found by Whelpdale and Shaw (1974) is also to be expected. For the generally more unstable summer conditions a higher  $\text{SO}_2$  deposition velocity would likely be appropriate. Barrie (personal communication) suggests a value of  $1 \text{ cm} \cdot \text{s}^{-1}$  with a factor two uncertainty. No summer measurements have been made at AOSERP for  $\text{SO}_2$  deposition velocity, nor have deposition velocities been determined for other gaseous pollutants.

Dry deposition of suspended particulates was investigated at Mildred Lake by Barrie (1978) using a Harwell Collector. These results for deposition velocity, for a short period of observation during June 1977, are given below:

Element	Deposition Velocity ( $\text{cm}\cdot\text{s}^{-1}$ )
Al	0.49
Ca	0.23
Mg	0.25
Mn	0.38
Particulate S	0.69
Ti	0.59
V	0.22

Note that, based on the deposition patterns, only vanadium and sulphur particulates measured at Mildred Lake are dominated by stack emissions, the remaining elements appearing to result primarily from wind-blow dust.

Data on wet deposition in the oil sands are available from a study by Barrie et al. (1978) conducted during June to August 1977. They give the following data for precipitation-weighted mean concentration of various precipitation constituents as follows:

Precipitation Constituent	Mean Concentration in Rain ( $\text{mg}\cdot\text{l}^{-1}$ )
$\text{SO}_4^{=}$ - S	0.13
$\text{Cl}^{=}$	0.47
$\text{NO}_3^{=}$ - N	0.04
$\text{NH}_4^+$	0.12
$\text{K}^+$	0.28
$\text{Na}^+$	0.06
$\text{Mg}^{++}$	0.08
$\text{Ca}^{++}$	0.08

Apparently no spacial pattern was evident, which may be the result of the complexity of the low-level airflow pattern for the convective precipitation conditions which dominate at this time of the year.

No results for wintertime wet-deposition are available.

### 3. THE ADPIC MODEL

#### 3.1 INTRODUCTION TO ADPIC

This chapter reviews two computer codes:

1. MATHEW, which uses a variational analysis procedure to analyse a three-dimensional mean wind field within the domain; and
2. ADPIC, which uses the winds from MATHEW along with parameterizations of wind fluctuations in a Particle-in-Cell approach to the definition of air pollution concentrations.

It is perhaps at first somewhat confusing to refer to both the total assessment methodology and the dispersion code as ADPIC. In practice the problem rarely arises owing to the context of the discussion.

A final brief section in this section discusses a rather simplified form of this package, PATRIC, which is finding wide application at LLL owing to its rapidity of execution.

#### 3.2 MATHEW

MATHEW is an acronym for "mass-adjusted three-dimensional wind field" model, developed at LLL, (Sherman 1978). The physical basis for the model is the conservation of mass in an incompressible fluid which is contained within a box bounded on the top and sides by (in general) open or "flow-through" boundaries and at the bottom by the surface of the Earth. Wind velocities within the fluid are adjusted by a minimal amount from an "observed" velocity field subject to the constraint of mass conservation. The "observed" field is itself derived from observations located sparsely within the model domain.

Mathematically, the conservation of mass in an incompressible fluid is represented by the equation of continuity (e.g., Haltiner and Martin 1957) which, using tensor notation becomes:

$$\frac{\partial u_i}{\partial x_i} = 0 , \quad (1)$$

where the Einstein summation convention is in effect unless otherwise noted (i.e., a repeated subscript indicates summation over the indices 1, 2, 3). In Equation (1),  $u_i = (u,v,w)$  is the three-component velocity vector and  $x_i = (x,y,z)$  are the three spatial dependent variables (x eastward; y northward; z vertical).

### 3.2.1 Aspects of the Calculus of Variations

Since the variational method is used by MATHEW and by the model MASCON to be described in Section 4.2 of this report, it seems appropriate to consider briefly the general variation method. The treatment here is abbreviated from Hildebrand (1962). A more detailed description is contained in Finlayson (1972).

The case of attempting to maximize or minimize an integral of the form:

$$I = \int_b^a G(x,u,u') dx, \quad (2)$$

where  $u' = \partial u / \partial x$  and  $u$  is a function of  $x$ , subject to appropriate boundary conditions at  $x = a$ ,  $x = b$ , is first considered. The problem is to find a function  $u(x)$  that maximizes (or minimizes, depending on the particular case) the integral,  $I$ , assuming that such a function indeed exists. The arguments which follow assume that all functions are differentiable to second-order so that all derivatives which appear are non-zero.

In Equation (2),  $u(x)$  is now replaced by  $u(x) + \epsilon \eta(x)$ , where the second term is the "variation of  $u(x)$ ", the function vanishes at the end points of the interval  $(a,b)$ , and the integral  $I$  is now denoted by  $I(\epsilon)$ . It can be shown that  $I$  is maximum (or minimum as the case may be) when  $I = I(0)$ : i.e., when the variation of  $u(x)$  is zero. Hence it follows that:

$$\frac{dI(\epsilon)}{d\epsilon} = 0 \quad (3)$$

When  $\epsilon = 0$ .

The result of applying Equation (3) is the Euler equation (sometimes called the Euler-Lagrange equation) associated with the problem of maximizing (or minimizing) the integral,  $I$  in Equation (2):

$$\frac{d}{dx} \left( \frac{\partial F}{\partial u'} \right) - \frac{\partial F}{\partial u} = 0 \quad (4)$$

The Euler equation may be expanded to a form which reveals it to be (in general) a second-order ordinary differential equation in  $u(x)$  which, in theory, may be solved for  $u(x)$  provided two boundary conditions of the form  $u(a) = A$ ,  $u(b) = B$  are applied. This then would be the solution to the problem posed in Equation (2).

A more general version of the above problem involves the imposition of an integral constraint in the form:

$$\int_b^a G(x, u, u') dx = K \quad (5)$$

where  $K$  is a prescribed constant. In this version, the function  $F$  in Equation (2) is replaced by:

$$H = F + \lambda G, \quad (6)$$

where  $\lambda$  is a Lagrange multiplier, an unknown constant which is to be determined. This Lagrange multiplier generally will appear in the Euler equation (4) and in its solution and is determined through use of Equation (5) and the two boundary conditions.

Further complications arise when, for example:

$$F = F(x_i, u_i, u_i') \quad (7)$$

i.e., a three-dimensional problem  $(x, y, z)$  with a three-component function  $u(x_i)$ ,  $v(x_i)$ ,  $w(x_i)$  and corresponding derivatives. The integral,  $I$ , is then taken over a volume and three Euler equations result. They are then solved for  $u$ ,  $v$ , and  $w$ .

In the particular case of the MATHEW model it will be seen that indeed Equations (5) and (7) are both involved. Fortunately, however, the formulation of the function,  $F$ , is sufficiently uncomplicated that the Euler equations are zeroth-order rather than second-order ordinary differential equations in  $u$ ,  $v$ , and  $w$ . Instead, difficulties arise in attempting to solve a second-order partial differential equation for  $\lambda$ . Once completed, however, obtaining the  $u_i$  field is quite straight forward.

### 3.2.2 The Variational Method Applied to MATHEW

Assuming that an "observed" wind velocity field,  $u_i^o = (u^o, v^o, w^o)$  has been derived from a set of (in general sparsely distributed) observations, the objective of MATHEW is to obtain an adjusted wind field  $u_i = (u, v, w)$  such that the variance of the difference between  $u_i^o$  and  $u_i$  is minimized subject to the strong constraint (i.e., a constraint which is to be satisfied exactly) that the adjusted field is non-divergent [i.e., satisfies Equation 1]).

In terms of Equation (2), the above objective can be expressed by the functional:

$$I(u_i, \lambda) = \int_V F(x_i, u^i) dx dy dz, \quad (8)$$

where the integration is over the entire model volume and

$$F = \alpha_i^2 (u_i - u_i^o)^2 + \lambda \left[ \frac{\partial u_i}{\partial x_i} \right] \quad (9)$$

with summation over repeated indices in each term. Here  $(x_i)$  is the Lagrange multiplier and

$$\alpha_i^2 \equiv \frac{1}{2} \sigma_i^{-2} \quad (10)$$

are Gauss precision moduli, where the values of the  $\sigma_i$  are observation errors and/or deviations of the observed field,  $u_i^o$  from the desired adjusted field,  $u_i$ . Hence the user of the model can subjectively determine the over-all degree of adjustment from the "observed" velocities based on his or her degree of faith in the observations or other criteria. In MATHEW it is assumed that  $\alpha_1 = \alpha_2$  as there is no apparent reason for distinction between the two horizontal components.

The Euler equations [see Equation (4)] associated with Equation (8) are as follows:

$$u_i = u_i^o + \frac{1}{2\alpha_i^2} \frac{\partial \lambda}{\partial x_i} \quad (\text{no sum on } i) \quad (11)$$

(consisting of one equation for each of the three values of  $i$ ) plus Equation (1). The equations are subject to the boundary conditions:

$$n_{x_i} \lambda \delta(u_i) = 0 \quad (\text{on the } x_i \text{ boundaries}) \quad (12)$$

where  $n_{x_i}$  is the outward positive unit normal of the direction  $x_i$  and  $\delta(u_i)$  is the variation of  $u_i$ .

An equation for  $\lambda$  is derived by differentiating Equation (11) and substituting the result in Equation (1):

$$\frac{\partial^2 \lambda}{\partial x^2} + \frac{\partial^2 \lambda}{\partial y^2} + \left[ \frac{\alpha_1}{\alpha_3} \right] \frac{\partial^2 \lambda}{\partial z^2} = -2\alpha_1^2 \left[ \frac{\partial u_i^o}{\partial x_i} \right] \quad (13)$$

Equation (13) is solved subject to the boundary conditions (12) and then the adjusted velocity field is solved using (11).

### 3.2.3 Boundary Conditions

An examination of Equation (12) shows that on the boundaries either  $\lambda = 0$  or the normal velocity component variation,  $n_{x_i} \delta(u_i) = 0$ . Specifying both over-determines the problem. Thus there are two types of boundaries corresponding to these two possibilities:

1. Open or "flow-through" boundaries on which  $\lambda = 0$  and thus, in general  $\partial\lambda/\partial x_i \neq 0$  in the direction normal to the boundary in question. Thus, from Equation (11) there is an adjustment of the velocity component normal to the boundary, implying a change in the amount of mass entering or leaving the model volume from that specified by the "observed" field.
2. Closed or "no-flow-through" boundaries on which  $\partial\lambda/\partial x_i = 0$  in the direction normal to the boundary in question. From Equation (11) this implies  $u_i = u_i^o$  for the component normal to the boundary. If the "observed" normal component is zero, as would be the case for a topographic boundary (or possibly a strong inversion layer), then the adjusted velocity field also would not permit mass transport across the boundary. Non-normal velocity components, however, are still free to adjust subject to the constraints in the same way as velocities at interior grid points.

### 3.2.4 Numerical Techniques

Equation (13) is approximated by using standard centered finite-differences in all three-dimensions at all interior points. At the boundaries, as discussed in the previous section, either

$\lambda = 0$  or  $\partial\lambda/\partial n = 0$  (where  $n$  is the normal direction). In the latter case the finite difference representation is:

$$\left. \frac{\partial\lambda}{\partial n} \right|_{\ell \pm 1} = \pm \frac{3\lambda_{\ell \pm 1} - 4\lambda_{\ell} + \lambda_{\ell \mp 1}}{2\Delta n} = 0 \quad (14)$$

where the point adjacent to the boundary is given by the index  $\ell$ , the differencing being forward or backward depending on the direction of the boundary from the point  $\ell$ .

The entire system of difference equations, representing Equation (13) at all grid points, is solved simultaneously for  $\lambda_{ijk}$  at each interior grid point using successive overrelaxation (Forsythe and Wasow 1960) with an overrelaxation factor of about 1.78. Since the resulting  $\lambda$  field must be numerically differentiated for use in Equation (11), the iterative procedure for the solution of Equation (13) is continued until there is sufficient significance in the solution to diminish as much as possible the truncation error associated with the numerical differentiation. In general, the allowable relative error in  $\lambda$  should be close to the computational precision of the particular computer being used.

The finite difference version of Equation (11) uses a centered difference for the derivative of  $\lambda$  (boundary values being obtained from Equation [14]) and a three-point smoother:

$$u_{ijk}^o = \frac{1}{4} \left( u_{i+1,j,k}^o + 2u_{i,j,k}^o + u_{i-1,j,k}^o \right) \quad (15)$$

for the observed  $u$ -field with corresponding equations for  $v^o$  and  $w^o$  involving the indices  $j$  and  $k$ , respectively.

### 3.2.5 Selection of Model Parameters

As the real topography is approximated by block topography in MATHEW, the complexity of the terrain and the requirements of the particular application determine the total dimensions of the model box and put upper limits on the grid sizes  $\Delta x_i$  in each of the three directions. These requirements of resolution and extent

of domain determine the minimum number of grid points required for model calculations. Provided that the resulting storage requirements are within the capacity of the computer and provided that the execution time would not be prohibitive, the application would then be feasible. Otherwise compromises would have to be made either on the extent of the domain under consideration or the resolution, or both.

Input parameters which have to be specified, if upper-level wind observations are not available, are the exponents in the power-law wind profile used in obtaining the "observed" velocities (Section 3.2.6). The values of the exponents depend on atmospheric stability.

Finally, the adjusted wind field will depend on the specification of the values  $\alpha_i$ , the Gauss precision moduli (ignoring for the moment their dependence on the "observed" wind field). As shown in Equation (10), if one assumes that the standard deviation of the observed field from the adjusted field is  $2 \text{ m.s.}^{-1}$  for the horizontal components than  $\alpha_1 = 0.5 \text{ m}^2 \text{ s}^{-2}$  (and  $\alpha_2 = \alpha_1$  as mentioned previously). According to Sherman (1978), the ratio  $(\alpha_1/\alpha_3)^2$  should be proportional to the expected magnitude of  $(w/u)^2$  or approximately  $10^{-4}$  assuming  $u \sim 10 \text{ m.s}^{-1}$  and  $w \sim 10^{-1} \text{ m.s}^{-1}$ .

### 3.2.6 Derivation of the Observed Wind Field

Typically the available observational data consist of measurements of horizontal wind velocity near the topographic surface, a synoptic analysis and, hopefully, one or more vertical profiles of horizontal wind velocity. Thus, in general the actual observations are rather sparsely distributed within the model volume. A scheme for derivation of the observed wind field,  $u_i$  at all grid points is needed before the main part of the MATHEW model, derivation of the adjusted field via the variational method as described above, may be applied.

Since measurements of vertical velocity are rarely available, MATHEW sets  $w^o = 0$  at all points. Experiments showed this to be a reasonable assumption in conditions of near-neutral atmospheric stability and, presumably, in regions unaffected by terrain slopes.

The spatially sparse surface measurements are adjusted from the height of observation,  $z_o$  to a height  $z$  using the power-law formula:

$$u_i^o = u_i^o(z_o) \left( \frac{z}{z_o} \right)^p, \quad i = 1, 2, \quad (16)$$

where  $p$  is determined by atmospheric stability conditions (Pendergast 1976) or from a least-squares fit to multiple-level tower data. According to Sherman (1978), Equation (16) is only used within the atmospheric surface layer. At the top of the model, horizontal winds are obtained from the synoptic analysis (e.g., either by interpolation in an objectively analyzed large-scale wind field or by obtaining the geostrophic wind from a mean sea level isobaric analysis or from the height field on a constant pressure chart). Vertical interpolation between the top of the surface layer and the top of the model follows the shape of a measured vertical wind profile, if available. Otherwise interpolation is used. In early versions of the model this was a linear interpolation but more recently this has been generalized to a form  $z^5$ .

Horizontal interpolation at the first grid level above local topography is accomplished (prior to vertical interpolation above the surface layer) by use of the nearest three observation points, the measurements being weighted inversely as the square of the distance from those points.

### 3.2.7 Data Requirements

Elevation of terrain is needed for purposes of definition of the block topography lower boundary. Experience at LLL indicates that the selection of topography is important; moving the grid point locations half a grid location can have a substantial influence on

the resulting flow field. This is a reflection of the aliasing problem; there should be no terrain in the model with wavelength less than two grid lengths. Naturally the resulting flow fields will not reflect these short wavelength influences which can be important for some conditions. For the AOSERP program the effects of the immediate Athabasca River trench cannot be resolved with the 1 to 5 km grid length commonly used in MATHEW.

Measurements of wind velocity at standard anemometer height are required at as many points as possible throughout the region of concern. As with topographic heights, these measurements should be representative of a fairly large area in the vicinity of the observation site. There should be a sufficient number of sites to resolve terrain-influenced variations in speed and direction. The location, elevation of terrain and anemometer height should be available for each site. An averaging time of the order of ten minutes would be appropriate although the shorter averaging periods typical of hourly observations are being employed with few problems.

A minimum of one vertical profile of wind velocity is required. Every additional profile is likely to provide the means for obtaining a better "observed" wind field, resulting in a more accurate adjusted non-divergent field and ultimately in improved calculations of pollutant concentration. Vertical resolution should be approximately the same as the grid-level spacing, which may be expected to be of order 50 m. The profiles should extend upwards for a minimum of about 100 m and preferably to the top of the boundary layer at a height of order 2 km or less. As in the case of surface measurements, averaging time should be of order 10 minutes. Shorter times may be allowable at greater heights due to the longer time scales which may be expected there. Vertical wind profiles may be obtained from instrumented towers in the lower part of the boundary layer, from pilot balloons (preferably tracked by double theodolite), from tethered balloons, or from an instrumented aircraft.

Information on atmospheric stability conditions is required for determination of the power-law exponent,  $p$  in Equation (16). It would probably be sufficient to have simply a Pasquill-Gifford stability category for this purpose. Detailed measurements of the vertical gradient of temperature are not necessary.

Finally, a synoptic analysis is required in order to obtain wind velocities at the top of the model box. The wind data may be interpolated at each model grid point from a larger scale objective analysis or they may be derived as geostrophic winds from a mean sea level pressure analysis or from, for example, an analysis of the height of the 85 kPa (850 mbar) pressure surface.

All of the above data should be observed quasi-simultaneously (e.g., preferably within a period of about 30 minutes; periods up to about one hour may perhaps be tolerated for upper parts of the boundary layer). The importance of good data at as many points as possible within the model volume cannot be overstressed. Although MATHEW is designed to derive reasonable winds from the "observed" data, its final output is strongly governed by the input observations. If these are poor and/or insufficient, there is little hope that MATHEW will accomplish more than a marginal improvement.

### 3.2.8 Computer Requirements

As noted above, the MATHEW code implemented at LLL is still in a research-development stage. The code has been written to take advantage of special compiler features available at LLL and is replete with non-standard FORTRAN features. Also the level of code documentation is low which also hinders conversion. For strict code conversion at least two man-months of skilled programmer effort would be required.

As implemented at LLL, the code takes advantage of the full capabilities of a LLL CDC 7600 computer. Storage usage is 57K small core memory (SCM), 470K large core memory (LCM) and 2M disk storage. Because of the limitations of the CDC 7600 computer

at CMC, the code would need to be restructured--about a three man-month effort for a skiller numerical analyst-programmer. Even so, array sizes would need to be reduced for operation at CMC. This could mean a reduction in grid resolution or area of coverage.

Additional programmer requirements would be about three man-months to restructure the graphic output and perhaps up to one man-year programmer-meteorologist time to generate input data-bases for the first case study, this latter figure including the complementary input for ADPIC.

Based on best estimates of comparative computer capabilities the AMTHEW code which executes in about two minues for a single analysis at LLL would require about 20 minutes at CMC.

### 3.2.9 Application and Verificiation

MATHEW has been applied to "eight different areas of the United States representing a variety of meteorological conditions and terrain features" (Sherman 1978). Two of the sites, results from which are discussed by Sherman, are located in Idaho and South Carolina. The former involved terrain elevation differences of over 1000 m between the highest and lowest points; at the latter the elevation difference was only 75 m.

In the Idaho study a grid of dimensions  $25 \times 33 \times 28 = 23\ 100$  points with a 4.3 km and 50 m spacing in the horizontal and vertical, respecitvely was used. Values of  $\sigma_1$  and  $\sigma_3$ , the global deviations of the observed field from the adjusted field for horizontal and vertical components, were taken to be 1 and  $0.01\ \text{m}\cdot\text{s}^{-1}$ , respectively. Surface layer depth was assumed to be 100 m (i.e.,  $2\Delta z$ ). Winds at the top boundary, rather than being derived from synoptic analyses, were assumed to be constant in the horizontal and obtained by interpolation in time from two vertical profile observations at one site. A value of  $p = 1/7$  was used in the power-law, Equation (16).

Results from the Idaho study showed that the adjusted field was non-divergent (magnitudes of order  $10^{-15}\ \text{s}^{-1}$ ) for all practical purposes. In the "observed" field the divergence was

about 11 orders of magnitude larger. Most of the adjustment appeared to have taken place near the topographic boundaries. One example of this adjustment was a cross-valley "observed" wind which was reduced in magnitude and the vertical component enhanced. Probably the fact that  $\alpha_1 = \alpha_2$  precluded a preferred treatment for either  $u$  or  $v$  at the expense of the other. Thus changes of horizontal wind direction appear to be, in general, not large except possibly at the site wall of a mountain or valley.

In the case of the South Carolina study, the available data were fewer (measurements at only three locations) and the meteorological situation more complicated (winds light and variable). Grid dimensions were  $51 \times 51 \times 15 = 39\,015$  points with horizontal and vertical spacing of 500 and 25 m, respectively. Sherman does not report the other input parameters and does not show any "observed" fields. The variational adjustment process, however, is stated to have resulted in overall rms changes at  $0.1$  to  $0.2 \text{ m.s}^{-1}$  and  $6$  to  $30^\circ$ . Although the terrain would appear to be less important than in the Idaho study, due to the fact that winds were light, the topographic boundaries may have exerted considerable influence on the wind direction in this case.

A general conclusion from the verification studies at LLL is that the model solution is rather sensitive to the topographic description given by the height input data. For example, shifting the grid one-half grid length could give a rather different flow field. Selection of an appropriate grid becomes a matter of experience. The model solution is similarly sensitive to the quality and quantity of input flow data.

### 3.2.10 Evaluation

Advantages and disadvantages of MATHEW are summarized in Table 6.

Table 6. Advantages and disadvantages of MATHEW.

ADVANTAGES	DISADVANTAGES
<p>More generally applicable than MASCON Gives full three-dimensional wind field</p>	<p>Precision moduli not dependent on stability</p>
<p>Permits accounting of observed data with adjustments in least-squares sense</p>	<p>Resolution of topography has important consequences for final flow field</p>
<p>Sufficient flexibility to handle non-textbook situations</p>	<p>Solution quality entirely dependent on having input data in sufficient quantity and quality</p>
<p>Will give solution with minimum input</p>	<p>Method of initial data interpolation subject to significant error in complex flow situations</p>
	<p>Model beyond the capacity of current CMC computer.</p>

From the point of view of model physics, the major concern is the assignment of precision moduli without respect to atmospheric stability. In a stable atmosphere one would expect much less adjustment in vertical velocity components than one would for the same guess field with an unstable stratification.

Of the problems arising the most overwhelming is the current lack of computer capacity in Canada to handle a problem of this magnitude.

### 3.3 ADPIC

ADPIC is an acronym for "atmospheric diffusion particle-in cell" model, developed by LLL (Lange 1978<sup>a</sup>). The physical basis for the model is the conservation of pollutant mass in an incompressible fluid with a specified non-divergent three-component velocity field. The model domain, in which mass conservation is required, is a box bounded on the top and sides by (in general) open or "flow-through" boundaries and at the bottom by the surface of the Earth. Although it must be specified as input from a model such as MATHEW (see Section 3.2), the wind field is, in general, a function of space and may also be time-dependent, usually by means of interpolation between two or more analysis times. The eddy diffusion coefficients used in the parameterization of the atmospheric diffusion processes are also specified functions of time and space. In practice, in ADPIC the horizontal eddy coefficient is a function of time and downwind distance along a pollutant plume axis (and hence a coefficient must be associated with each source), while the vertical eddy coefficient is a function of height alone. Provision is also made for variation of surface roughness in space, for wet and dry deposition of pollutants at the surface and for radioactive decay, when applicable.

Mathematically, ADPIC attempts to solve the nonlinear transport-diffusion equation for a pollutant which, in tensor notation, is expressed:

$$\frac{\partial \chi}{\partial t} + U_{A_i} \frac{\partial \chi}{\partial x_i} = \frac{\partial}{\partial x_i} \left( K \frac{\partial \chi}{\partial x_i} \right) \quad (17)$$

where  $\chi$  is a scalar pollutant concentration,  $U_{A_i}$  is the  $i$ th component of the given non-divergent advection velocity and  $K$ , the eddy diffusion coefficient is as follows:

$$K_h(s,t) = \bar{U} \sigma_y \frac{d \sigma_y}{ds} \quad (18a)$$

$$\sigma_y(s) = a s^b \quad (18b)$$

for  $i = 1, 2$  (the horizontal diffusion), and in the surface layer

$$K_z(z) = \frac{ku_*z}{\phi_M(z/L)} \quad (18c)$$

while in the remainder of the boundary layer

$$K_z(z) = \left( \frac{z}{h} \right)^\beta \exp \left[ - \left( \frac{z}{h} \right)^\alpha \right] u_* \left( \frac{h}{L} \right)^\delta \quad (18d)$$

for  $i = 3$  (vertical diffusion). In the above equation,  $\bar{U}$  is the local mean wind ( $m \cdot s^{-1}$ ),  $\sigma_y$  is the horizontal dispersion coefficient normal to the flow (m),  $s$  is distance along the plume axis (m),  $z$  is height above the surface (m),  $h$  is boundary layer height (m),  $L$  is Monin-Obukhov length (m),  $k$  is the von Karman constant,  $u_*$  is friction velocity,  $\phi_M$  is the non-dimensionalized wind shear, and  $a, b, \beta, \alpha, \delta$  are constants for any particular stability case.

### 3.3.1 Eulerian-Lagrangian Particle-in-Cell Method

Making use of the fact that in Equation (17) the  $U_A$  field is non-divergent, i.e.,

$$\frac{\partial U_{A_i}}{\partial x_i} = 0 \quad (19)$$

Equation (17) may be written as:

$$\frac{\partial \chi}{\partial t} = - \frac{\partial}{\partial x_i} (\chi U_{P_i}) \quad (20)$$

where

$$U_{P_i} = U_{A_i} + U_{D_i} \quad (21)$$

is the pseudo-transport velocity, composed of the sum of the non-divergent advection velocity and a diffusivity velocity,

$$U_{D_i} = - \frac{K}{\chi} \frac{\partial \chi}{\partial x_i}, \quad \chi \neq 0 \quad (22)$$

As before  $K = K_h$  for  $i = 1, 2$  and  $K = K_z$  for  $i = 3$  (Equation 18). Inherent in the arrangement of the equations in this form is the assumption of non-zero concentrations. Note that the argument used in formulating diffusivity velocity is analogous to that used for deposition velocity.

Solution of Equation (2) is performed in two steps, the first Eulerian and the second Lagrangian as follows:

1. Eulerian step: Concentrations,  $\chi \neq 0$  and the eddy coefficients,  $K(x_i, t)$  are used to calculate diffusivity velocities from Equation (22) on a three-dimensional grid. Then Equation (21) is applied to obtain pseudo-transport velocities.

2. Lagrangian step: If  $R_i(t) = (R_1, R_2, R_3)$  are the co-ordinates of a given particle at time,  $t$ , then the rate of change of co-ordinates is given by the Lagrangian equivalent of Equation (20), viz.,

$$\frac{\partial R_i}{\partial t} = U_{p_i} \quad (23)$$

Equation (23) is used to obtain new co-ordinates of each particle. Finally a new concentration field,  $\chi$ , is obtained from the new co-ordinates by counting the number of particles within each Eulerian grid cell.

It should be noted that, in addition to its co-ordinates, each particle may be given one or more of the following properties: age since generation, mass, activity, species, and size. These properties may be used in a parameterized computation of wet and dry deposition, radioactivity decay, reaction rates and particle size distributions of pollutants.

### 3.3.2 Boundary Conditions

Equation (20) requires a specification of  $\chi^U_{pn}$  or its derivative with respect to  $\chi_n$  ( $n$  indicating the component normal to the boundary). Usually at lateral and upper boundaries the derivative is set equal to zero, implying that inflow and outflow of particles are permitted. Reflection at an inversion "cap" or the topographic boundary is accomplished by choosing a value  $\chi^U_{pn} = 0$ , corresponding to zero mass flux. Deposition can be simulated by specification of  $\chi^U_{pn}$  equal to a deposition velocity.

In the solution of Equation (23), if the new co-ordinates indicate that a particle has left the model domain, there are three possible treatments according to which type of boundary conditions exists:

1. The particle is "annihilated" in the case of flow-through boundaries;

2. The particle is reflected and appropriate new co-ordinates determined in the case of a reflecting boundary; and
3. The particle is deposited on the surface if a deposition velocity has been specified.

### 3.3.3 Numerical Techniques

The Eulerian grid used for numerical calculations is coded to represent rectangular parallelepiped cells of uniform size. Concentrations are defined at cell centres and all velocities and eddy coefficients at cell corners. Locations of particles are defined by their co-ordinates,  $R_i$ , within the grid. Assuming that the center of a given cell has integer co-ordinates  $(l, k, j)$  then velocities and eddy coefficients are defined at the point  $(l+\frac{1}{2}, k+\frac{1}{2}, j+\frac{1}{2})$ . In this staggered grid the appropriate finite difference representation of Equation (22) is:

$$U_{D_i}^{l+\frac{1}{2}, k+\frac{1}{2}, j+\frac{1}{2}} = \frac{-K^{l+\frac{1}{2}, k+\frac{1}{2}, j+\frac{1}{2}}}{\Delta x_i} \frac{D^{l+\frac{1}{2}, k+\frac{1}{2}, j+\frac{1}{2}}}{S^{l+\frac{1}{2}, k+\frac{1}{2}, j+\frac{1}{2}}} \quad (24)$$

co-ordinates are shown as superscripts,  $S$  is the average of the concentrations of the eight cells which meet at the specified corner and  $D$  is the average of the difference between concentrations in the four pairs of those same cells taken in the direction,  $x_i$ . For example when  $i = 1$ , differences are taken between points at which the first superscript is  $l+1$  and  $l$ , respectively, and the four pairs each have a second superscript  $k+1$  or  $k$  and a third superscript  $j+1$  or  $j$ . Lange (1978<sup>a</sup>) who shows Equation (24) projected onto one dimension, indicates that this finite difference representation of Equation (22) avoids the problem of division by zero concentrations that would arise in a non-staggered grid. this should be regarded as a convenient numerical artifice which avoids problems when  $\chi = 0$  rather than a fundamental solution.

By assuming a Gaussian concentration distribution with a standard deviation of  $\sigma$ , Lange shows that the finite difference scheme used in Equation (24) is second-order and that the relative error in one dimension, retaining only the first term is:

$$RE = \left( \frac{\Delta x}{2\sigma} \right)^2 \quad (25)$$

indicating that for accurate results one should choose the cell size  $\Delta x \ll 2\sigma$ .

In practice, with a fixed cell size this criterion cannot be satisfied near a point source and a special treatment is needed.

In effect an assumption is made about the initial distribution of particles from the source (usually Gaussian) and the diffusivity velocities calculated based on particular position within that distribution until the spread is great enough to be resolved by the Eulerian grid mesh. For simplicity consider the case of one-dimensional dispersion in the y direction. For a Gaussian distribution the concentration field is

$$\chi = \frac{Q}{(2\pi)^{\frac{1}{2}} \sigma_y} \exp \left( -\frac{1}{2} \frac{y^2}{\sigma_y^2} \right)$$

with the usual notation. For the definition of diffusion

$$\text{flux } \chi U_D = -k_y \frac{\partial \chi}{\partial y}$$

$$\text{so that } U_D = -k_y \frac{\partial \ln \chi}{\partial y}$$

substituting for  $\chi$  gives

$$U_D = \frac{k_y y}{\sigma_y^2}$$

It remains to make a convenient choice of  $K_y$  and  $\sigma_y$  from amongst the several available. This prescription of diffusivity velocity avoids the requirement to specify  $\chi$  and its gradient from the Eulerian mesh. Extended further downwind it is the parameterization of diffusivity velocity used in the PATRIC code described in Section 3.4.

The finite difference representation of Equation (23), correcting a typographic error in Lange's Equation (3), is:

$$R_i(t+\Delta t) = R_i(t) + U_{p_i} \Delta t \quad (26)$$

a forward-stepping explicit scheme.

A numerical expedient assigns a fictitious volume to each particle of the same dimensions as the basic Eulerian grid cell. In calculating the concentration field each particle contributes some fractional part of its weight to eight nearest-neighbour cells in proportion to the overlap of its volume with the cell volumes. The effect is to smooth the concentration field and thus the diffusivity velocity field. A saving in the number of particles that need to be followed results.

#### 3.3.4 Data Requirements

ADPIC requires as input a non-divergent three-dimensional, three-component wind velocity field, provided by a model such as MATHEW. In this respect the data requirements of ADPIC are the same as those of MATHEW (Section 3.2.7). For time-dependent problems, the wind field must be available at two or more times, usually at intervals of the order of one hour. Interpolation in time gives a trial wind field at the current timestep. Possibly MATHEW would have to be applied to this trial field in order to ensure non-divergence. For a problem concerning the continuous release of pollutant, source emission rate and effective source height are

needed in order to determine the co-ordinates of new particles as they are emitted. Effective source height depends on certain stack parameters such as stack diameter, exit velocity and stack gas temperature. Atmospheric temperature at stack height is also needed.

In addition, information on which to base the diffusivity velocity parameterization is needed. The formulation at LLL is flexible enough to use a Pasquill category as an information minimum or detailed turbulence information if it is available. Naturally the sophistication of the input is reflected in the quality of the output.

### 3.3.5 Computer Requirements

As with the MATHEW code, the ADPIC code is written in the LRLTRAN version of FORTRAN and as the code is largely undocumented at least two man-months of effort would be required for code conversion. However, with the core limitations of CMC and the unique particle-in-cell nature of the technique making restructuring using overlays virtually impossible, a complete rewriting of the program would be required. A programmer-analyst assigned to this model would require one man-year to complete the task. This being the case it is extremely difficult at this junction to estimate run times--something of the order 10 minutes execution time per simulated hour. This technique has the advantage of being susceptible to vectorization and, if this is practicable, run times could be reduced by a factor of two.

### 3.3.6 Application and Verification

Comparison of ADPIC results with analytic solutions for simple, linearized cases with Gaussian pollutant distributions were performed, as reported in Lange (1978<sup>a</sup>), in order to verify the model's computer coding. Results apparently agreed to within 5% of the true values over regional scales of order 100 km and time scales of several hours. Since these test cases are very much

simplified versions of actual atmospheric conditions, their success does not represent a full verification of the model.

The ADPIC model was applied to the two sites in Idaho and South Carolina where MATHEW was tested (Section 3.2.9). In the Idaho study, both observations and ADPIC showed a double peak in concentration at the location of one of the pollution samplers, the double peak being attributed to temporal changes in the regional flow field and as an effect of topography. In that sense, ADPIC performed much better than the Gaussian plume model which, of course, only showed one peak. However, the time of plume passage over the site was one to two hours later (depending on which peak is used) in the ADPIC results than in the field measurements. Calculated concentrations across the plume ranged from being quite accurate at the plume edges to about one order of magnitude low near the plume peaks. The Gaussian plume model gave a much better estimate of maximum concentration but in a plume which was much too narrow.

Lange (1978<sup>a</sup>) summarizes results of both field studies by saying that "typically, 60% of the time ADPIC was within a factor of 2 of field data while 96% of the time it agreed to within an order of magnitude". The potential user of ADPIC would have to decide whether errors,

$$r = \frac{\text{ADPIC Values}}{\text{Measured Values}}$$

between 0.1 and 10 can be tolerated in the particular application of concern. Lange (1978<sup>a</sup>) does say that in the above applications the model parameters were not tuned to the particular site, type of pollutant source or sampling method. Hence some improvement in error statistics could be expected after application to the AOSERP site and comparison with sampling data as mentioned in Section 3.3.4.

### 3.3.7 Evaluation

Advantages and disadvantages of ADPIC are summarized in Table 7.

The predominant problem is the practical one of required computer resources. These effectively eliminate the model as a candidate for AOSERP application at present. Even with the vast computer capacity at LLL it does not appear feasible to apply the model for reactive photochemistry problems.

Lange (1978<sup>a</sup>) reports that with no initial concentrations the model is most sensitive to errors in wind direction, topography, diffusion parameters, source strength, and wind speed, in that order.

### 3.4 PATRIC

PATRIC is a simplified and speeded-up version of the ADPIC code. The temporal evolution of the particle distribution results from transport due to advection by a defined wind and diffusivity velocity derived by assuming a Gaussian concentration profile.

The advective wind field is supplied by interpolating station values of speed and direction and, for more rapid execution, is used directly as such. In this manner false local divergence and convergence patterns occur. They are not eliminated as in MATHEW, but pollutant mass is conserved owing to the particle-in-cell nature of the procedure. The terrain is assumed flat, so that its effect does not enter the calculation except inasmuch as its effects are in the input wind observations.

The parameterization for diffusivity velocity is as described in Section 3.3.3 for the region in ADPIC where the typical plume dimension is less than the grid length. The formulation is described in more detail in Lange (1978<sup>b</sup>). One apparent problem with this formulation is the potential accounting for the effect of vertical variation of wind (speed and direction) twice as it is incorporated explicitly in the specified wind field and

Table 7. Advantages and disadvantages of ADPIC.

ADVANTAGES	DISADVANTAGES
Formulation easily takes into account decay and deposition processes	Diffusion velocities calculated from standard sigmas and the Gaussian assumption may need to be applied to considerable downwind distances, depending on rate of spread and grid length.
Avoids numerical diffusion problems of finite difference formulations	Definition of initial concentrations strongly influences solution until this pollutant advected out of region of interest
More generally applicable than LIRAQ-1	Not formulated for reactive photochemistry or wet-deposition
Code subject to vectorization to speed execution on vector computers.	Requires computer capacity beyond current Canadian capabilities.

implicitly in the dispersion coefficient curves used in the diffusivity velocity computation. The problem is currently under investigation at LLL.

Lange (1978<sup>b</sup>) gives an example of a typical PATRIC simulation. A region of 100 x 100 km (similar to the AOSERP area) is simulated to a height of 1 km. The typical grid mesh is 10 x 10 x 5 cells. Continuous sources are modeled by a sequence of Gaussian puffs, one each time step. Run time on the LLL CDC 7600 computer was about 1 to 2 minutes for a 1-day simulation. Core utilization is 30K SCM, 250 LCM, and 3 MW disk. Although these are beyond the capability of the CMC 7600 computer, it appears likely that, with an extensive rewrite, the PATRIC model could be operated on the CMC machine.

Since PATRIC is based on the ADPIC formulation, it is verified for certain simple cases by the ADPIC verification. According to Lange, PATRIC has been run successfully for a set of advection fields based on hourly winds from stations in the San Francisco Bay area for a typical month to give time-integrated air concentrations and deposition from a simulated pollution source. Also, an annual wind set was investigated for more long-term dispersion patterns for an area around the Dupont Savannah River Plant in South Carolina. PATRIC is also being applied on a real-time basis at LLL in the prediction of dispersion from accidental emissions such as those from the recent return to earth in Canada of a USSR nuclear-powered satellite.

In view of the inordinate computer requirement needed for the MATHEW and ADPIC code application, PATRIC appears to be an attractive alternative for AOSERP. As noted above, however, the implementation would not be easy on the CMC system and there remain some aspects of the physics of the model which require further clarification. Studies to resolve these problems would need to proceed on a research and development basis, at least for the initial phase.

#### 4. THE LIRAQ MODEL

##### 4.1 INTRODUCTION TO LIRAQ

The Livermore Regional Air Quality (LIRAQ) model was developed by LLL as an operational tool to assist air quality control agencies in tasks such as assessing the compliance of present ambient air quality with Federal standards, evaluating the impact on regional air quality of various land use alternatives, and predicting the effect on regional air quality of new sources and postulated emission control strategies.

LIRAQ was developed for the study of time-dependent regional air quality in the San Francisco Bay area which is characterized by complex topography, frequent occurrence of capping inversions, numerous pollutant sources (area, line, and point), and important photochemical pollutant transformations. Two critical assumptions are made to reduce this problem to manageable proportions. Firstly, it is assumed that there is no effect of air quality on the meteorological fields beyond that contained in the meteorological observations. This simplification allows an independent analysis of the meteorological fields to be made and then applied for different emission scenarios. In this way the treatment of the meteorological fields is diagnostic, while that of the pollution fields is predictive.

The second major assumption is that only a single vertical layer, between the surface and the elevated inversion, is treated. The height of the surface can change in space due to topography and the inversion height is allowed to vary with space and time. Because an elevated inversion is a common occurrence in the Bay area for conditions of regional air quality concern this is an appropriate and useful assumption there.

With the above simplification the LIRAQ model is capable of simulating the time and space varying concentrations of non-reactive and reactive pollutants on a regional basis using prescribed

meteorology and source emissions. MacCracken (1975) notes the following limitations of the model's applicability (i.e., situations in which it is inappropriate):

1. Air quality problems at short range (less than several kilometres) from major point sources;
2. Air quality problems close to intense line sources such as highways;
3. Air quality problems affected by the presence of major buildings or obstructions (e.g. street, canyons);
4. Air quality problems involving emissions from natural sources, unless they are included in the source emission inventory;
5. Air quality problems affected by species not in the model; and
6. Air quality problems that depend strongly on distribution of pollutants in the vertical (e.g., effects of varying stack heights).

The basic information flow for LIRAQ is shown in Figure 3 in a simplified form. When the LIRAQ program is initiated it runs interactively with an operator seated at an input device (TTY) who supplies a variety of run data. This interactive phase allows the operator to attach various data library files to the program, modify these files as appropriate, and generally provide the program the input information it needs:

1. Geographic data (QGEO) is the area of interest on an appropriate grid and its topography;
2. Pollution source data library inputs (area, line or point sources), QSOR, are supplied for the location and temporal variation for each pollutant species.
3. Meteorological data library inputs (QTRAN) are analysed by the program MASCON for the scenario of interest and stored as meteorological files of grid point data;

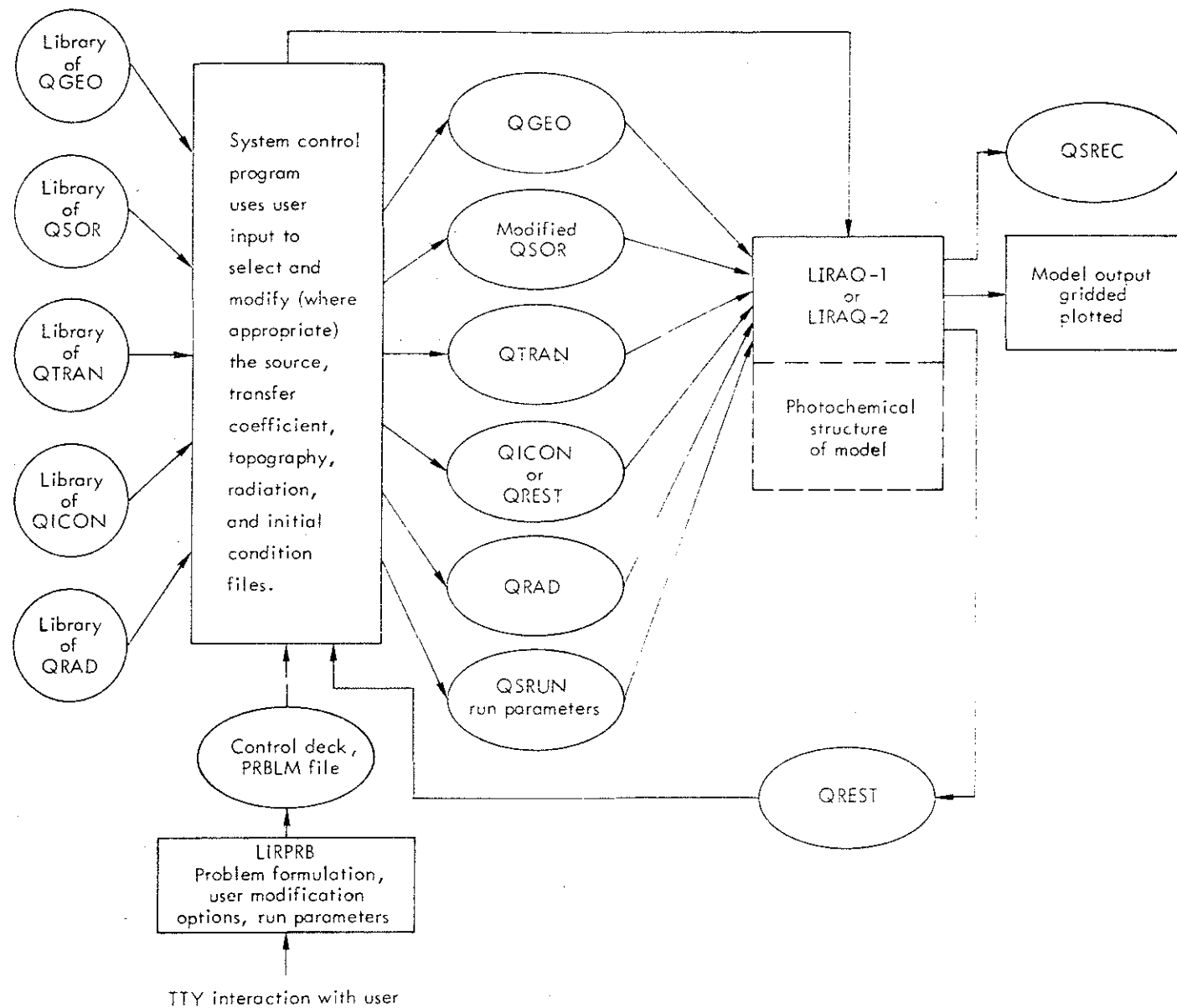


Figure 3. Basic information flow for LIRAQ.

4. Data on the initial time pollution concentrations (QICON) are required for each grid point. The program has provisions for analyzing observed pollution data or using the result of a previous simulation, QREST (restart pollution concentration file); and
5. Finally, for LIRAQ-2 only, data on solar radiation (QRAD) from a network of radiometers are required to feed to the photochemical equations.

Good quality input data are prerequisites for reliable methods.

After the initialization phase LIRAQ proceeds to a prognostic phase where the advections, eddy transports, depositions, chemical transformations, and source additions of pollutants are computed using finite difference algorithms. As simulated time progresses, new fields of pollution source data and meteorological data are introduced into the calculations to reflect their temporal variation.

Periodically model outputs in tabular, graphical and computer compatible (QSREC) form are produced. Analysis of the voluminous data from a model run is akin to the problems of data analysis of a large field experiment, with the exception that (hopefully) the data are better organized and complete. Typically output formatting, especially for graphics, occupies the same order of computer time as the pollution prediction phase.

Further more detailed considerations of the above considerations are available in MacCracken (1975). In the remainder of this section we proceed to consider in more detail the particularly unique elements of this model. Section 4.2 discusses the MASCON model which provides the meteorological flow field data for the model. In Section 4.3 the LIRAQ-1 model, which considers only non-reactive pollutants, is discussed. LIRAQ-2 which treats photochemistry is discussed in Section 4.4.

## 4.2 MASCON

MASCON is a diagnostic numerical model which provides mass consistent meteorological input to LIRAQ. Because LIRAQ employs only a single vertical layer (bounded by the surface and an elevated inversion), the formulation is somewhat simpler than for MATHEW. Figure 4 shows a schematic flow chart of the input and output files used by MASCON, as implemented by LLL.

The Run Specification input includes a problem title, beginning and ending dates and times, and a specification of the area of interest and grid size. MASCON is configured to run for up to 48 hours simulation time on grids up to 65 x 65 with grid sizes of 1, 2, or 5 km.

Topographic data are available to MASCON at 1 km grid intervals. For coarser resolution runs, data are selected at the appropriate intervals without any averaging. Thus the possibility of aliasing errors needs to be taken into account when selecting the grid sizes. Spatial averaging of topography would be a better approach. Geographical locations of all meteorological and air quality stations in the area are also input to MASCON.

For a typical LIRAQ case study at LLL an analysis of the meteorological fields is required at 3-hour intervals. Observational data for MASCON are typically available at 30 locations within the domain. Six input data formats are recognized in every three-hourly input cycle:

1. MSL inversion base height by station location;
2. MSL inversion base height by Universal Transverse Mercator (UTM) co-ordinate location;
3. Surface vector wind by station location;
4. Mean layer vector wind and inversion base height by station location;
5. Surface vector wind by UTM co-ordinate location; and
6. Mean layer vector wind and inversion base height by UTM location.

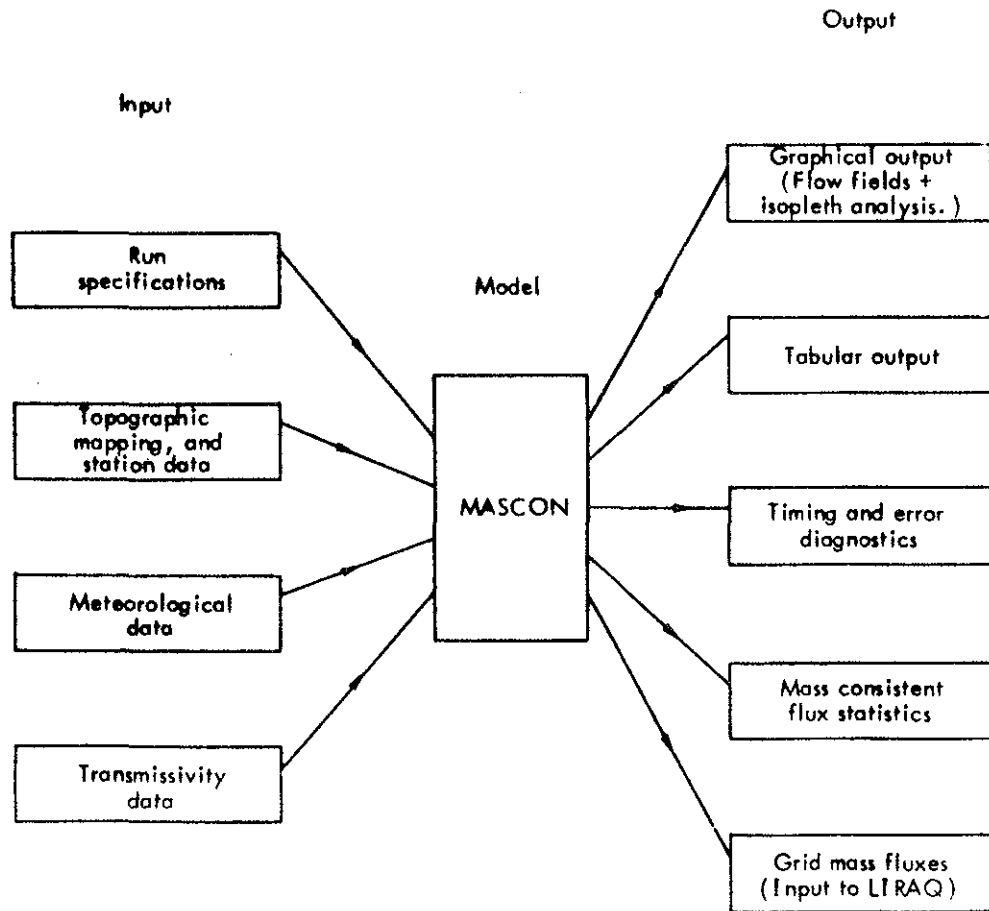


Figure 4. Basic information flow for MASCON.

Additional details concerning the manipulation to these data to obtain observed fluxes are given in a later section.

Transmissivity data input is required by LIRAQ-2 for input to the photochemical model.

Using these data the MASCON model itself adjusts the mass flux (product of mean wind and thickness of sub-inversion layer) together with the vertical velocity and inversion base to provide complete fields of these parameters which are consistent with both the equation of continuity (equivalent to the conservation of mass for an incompressible fluid) and the limited set of observational data.

The basic output from MASCON is grid point mass fluxes in computer compatible form for direct input to LIRAQ. In addition numerous other presentations of the analyses can be obtained to enable rapid checking. At LLL this checking is considered an important enough task to devote about as much computer time to producing readily interpretable graphical output as in performing the actual analysis.

The detailed discussion of MASCON that follows is based on a recent paper by Dickerson (1978), a report by MacCracken (1975), and discussions with LLL personnel.

#### 4.2.1 Physical Basis

Because of the formulation of LIRAQ in flux form it is necessary to provide these models meteorological fields which satisfy the mass continuity constraint, as for MATHEW;

$$\frac{\partial u_i}{\partial x_i} = 0 \quad (27)$$

LIRAQ uses the formulation of a well-mixed sub-inversion layer, height  $h$  above topography, so that only layer mean mass fluxes

are required. Integrating from the surface to inversion base and writing in flux form for the horizontal components

$$\frac{\partial h \bar{u}}{\partial x} + \frac{\partial h \bar{v}}{\partial y} + \int_0^h \frac{\partial w}{\partial z} dz - \bar{u} \frac{\partial h}{\partial x} - \bar{v} \frac{\partial h}{\partial y} = 0, \quad (28)$$

where  $\bar{u}$  and  $\bar{v}$  are layer mean winds. The third term is approximated  $h(w_T - w_B)/h$  where  $w_T$  and  $w_B$  are the vertical velocities at the top and bottom of the sub-inversion layer respectively. While  $w_B = 0$  (at the surface) this term becomes simply  $w_T$ . The final two terms can be re-expressed in terms of the rate of inversion height change

$$\frac{dh}{dt} = \frac{\partial h}{\partial t} + \bar{u} \frac{\partial h}{\partial x} + \bar{v} \frac{\partial h}{\partial y}.$$

On assuming that  $dh/dt = 0$ , so that at any point advective changes in inversion height are dominant over other causes such as local heating, not always a good assumption,

$$\frac{\partial h}{\partial t} + \frac{\partial h \bar{u}}{\partial x} + \frac{\partial h \bar{v}}{\partial y} + w_T = 0,$$

or writing for the fluxes

$$U = h \bar{u}, \quad V = h \bar{v}$$

$$\frac{\partial h}{\partial t} + \frac{\partial U}{\partial x} + \frac{\partial V}{\partial y} + w_T = 0. \quad (29)$$

MASCON adjusts the variables  $U$ ,  $V$  and  $w_T$  so as to satisfy Equation (29) while remaining consistent with available observations.

#### 4.2.2 Mathematical Basis

When observational data are placed in the mass continuity equation it is normally observed that the equality is not satisfied as there is a residual  $\epsilon_o$ .

$$\left( \frac{\partial h}{\partial t} \right) + \frac{\partial U_o}{\partial x} + \frac{\partial V_o}{\partial y} + w_T = \epsilon_o$$

The variational formulation, as detailed in the discussion of MATHEW, requires the minimization of the variational function

$$E = \int_{x,y} \left[ \alpha_1^2 (U - U_o)^2 + \alpha_1^2 (V - V_o)^2 + \alpha_3^2 (w_T - w_{T_o})^2 + \lambda \left( \frac{\partial h}{\partial t} + \frac{\partial U}{\partial x} + \frac{\partial V}{\partial y} + w_T \right) \right] dx dy$$

where  $\alpha_1, \alpha_3$  are Gauss precision moduli and  $\lambda(x,y)$  the Lagrangian multiplier. Zero subscript indicates an observed value. The Euler-Lagrange equations associated with the minimization are

$$\frac{\partial^2 \bar{\lambda}}{\partial x^2} + \frac{\partial^2 \bar{\lambda}}{\partial y^2} - \left( \frac{\alpha_1}{\alpha_3} \right) \bar{\lambda} + \left( \frac{\partial h}{\partial t} \right)_o + \frac{\partial U_o}{\partial x} + \frac{\partial V_o}{\partial y} + w_{T_o} = 0 \quad (30)$$

where

$$\begin{aligned} U &= U_o + \frac{\partial \bar{\lambda}}{\partial x} \\ V &= V_o + \frac{\partial \bar{\lambda}}{\partial y} \\ w_T &= w_{T_o} - \left( \frac{\alpha_1}{\alpha_3} \right)^2 \bar{\lambda} \end{aligned}$$

and by definition

$$\bar{\lambda} = \frac{1}{\alpha_1} \frac{\lambda}{2}$$

The solution is obtained by solving (30) by successive over-relaxation for  $\bar{\lambda}$  with observed values  $U_o$ ,  $V_o$ ,  $w_{To}$  and  $(\partial h / \partial t)_o$ , and then substituting to obtain the adjusted values  $(U, V, w_T)$ .

#### 4.2.3 Boundary Conditions and Constraints

In order to solve the governing equation it is necessary to make a specification about the Lagrangian multiplier around the boundary of the domain. The Dirichlet condition  $\lambda = 0$ , which permits the flux component normal to the boundary to vary while constraining the parallel component and vertical velocity to retain their "observed" boundary values, was found successful in producing reasonable looking fields. An additional Neumann constraint on  $\lambda$  is required at some locations at the interior of the domain where the topography rises through the inversion (in practice applied where the inversion base height is less than 50 m above topography). In this case the normal flux components is constrained to zero so that there is no airflow beneath the surface.

Only the ratio  $\alpha_1/\alpha_3$  needs to be specified rather than the individual Gauss precision moduli. Examination of the variational function shows that as  $\alpha_1/\alpha_3 \rightarrow 0$  the adjustment of the horizontal fluxes is maximized, while as  $\alpha_1/\alpha_3 \rightarrow \infty$  the adjustment is greater in the vertical velocity. In application at LLL a value  $(\alpha_1/\alpha_3)^2 = 10^{-9} \text{ m}^{-2}$  is employed.

#### 4.2.4 Computational Formulation

To solve the elliptic P.D.E. for  $\lambda$  a finite difference grid is used to approximate the equation. Figure 5 shows the staggered grid arrangement employed.

Firstly an analysis of observed meteorological data for  $u$ ,  $v$ , and  $h$  is made at the grid points represented by solid

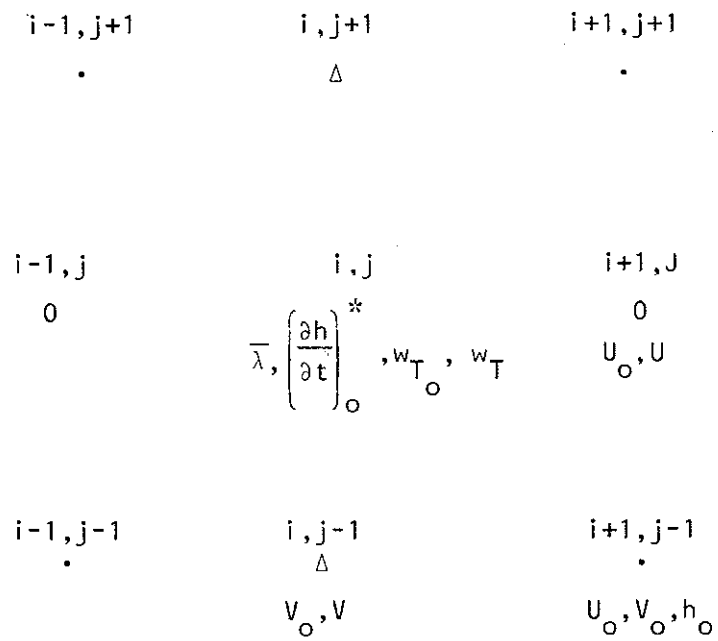


Figure 5. Staggered finite difference grid for the MASCON relaxation.

dots. For velocity this is done employing a distance weighted average of the three closest observations to the grid point

$$V_o = \frac{\sum_{i=1}^3 V_i \exp(-0.1 r_i)}{\sum_{i=1}^3 \exp(-0.1 r_i)}$$

where  $v$  is the calculated east-west or north-south grid point layer mean velocity component and  $v_i$  and  $r_i$  are the corresponding "observed" layer mean velocity components and distances. For inversion base height there are typically only a few observations available in the Bay area. Subjective analysis is used incorporating these observations and a considerable base of climatological knowledge accumulated from previous area studies. This is one of the weaker aspects of the procedure.

The fields are next interpolated to the intermediate points, open circles for  $U_o$ , open triangles for  $V_o$ , using interpolation between the two adjacent solid dot points and the flux definitions  $U_o = u_o h_o$ ,  $V_o = v_o h_o$ .

The value of  $(\partial h / \partial t)_o$  is determined by subtracting  $h_o$  values analysed at successive three-hourly times and interpolating to the star grid point from the four surrounding points. Again, this is a weakness of the procedure since it involves taking a difference of two poorly defined quantities. Also it will likely give a  $(\partial h / \partial t)_o$  value which is inconsistent with the assumption  $dh/dt = 0$  used in deriving Equation (29). These problems do not appear to have been investigated in depth as far as their impact on LIRAQ results is concerned.

The value of  $w_{T_o}$  is set to zero as MASCON results appear insensitive to this initial choice.

To finite difference form the last four terms in Equation (3) are written

$$\epsilon_o = \left( \frac{\partial h}{\partial t} \right)_o + \left( \frac{U_o \text{ } i+1, j - U_o \text{ } i-1, j}{2\Delta x} \right) + \left( \frac{V_o \text{ } i, j+1 - V_o \text{ } i, j-1}{2\Delta y} \right)$$

so that using centred differences for the flux derivatives

$$\frac{\bar{\lambda}_{i-1,j} + \bar{\lambda}_{i+1,j-1} + \bar{\lambda}_{i,j-1} + \bar{\lambda}_{i,j+1} - 4\bar{\lambda}_{i,j}}{4\Delta x^2} - \left(\frac{\alpha_1}{\alpha_3}\right)^2 \bar{\lambda}_{i,j} + \epsilon_0 = 0$$

Successive over-relaxation is used to solve this equation. Initial guess values of the  $\bar{\lambda}$ 's are put into the above equation to calculate an adjustment to  $\lambda_{i,j}$  so that the equation is satisfied

$$D_{i,j} = \frac{\epsilon_0 + \frac{\bar{\lambda}_{i-1,j} + \bar{\lambda}_{i+1,j} + \bar{\lambda}_{i,j-1} + \bar{\lambda}_{i,j+1}}{4\Delta x^2}}{\left[ \frac{1}{\Delta x^2} + \left(\frac{\alpha_1}{\alpha_3}\right)^2 \right]} - \bar{\lambda}_{i,j}$$

A new  $\bar{\lambda}_{i,j}$  value  $\bar{\lambda}_{i,j}^*$  is calculated according to

$$\bar{\lambda}_{i,j}^* = \bar{\lambda}_{i,j} + R D_{i,j}$$

Experience shows that if R is chosen slightly greater than 1 the convergence is expedited. Convergence is assumed after repeated adjustments when the maximum residual in the continuity equation is approximately  $10^{-6} \text{ m.s}^{-1}$ .

#### 4.2.5 Data Requirements

There are a number of observing systems which can provide input meteorological data for analysis by MASCON. These systems can provide both the mean layer wind components and inversion base heights required.

1. Minisonde and Rawinsonde systems can provide these data by straight-forward analysis of the soundings. Since the observation sites are usually fixed the appropriate input format is "mean layer vector wind and inversion based height by station location".

These systems are relatively reliable, allow for reasonably frequent soundings ( $\sim 20$  min) and data can become available in near real time. However, to obtain spatial resolution a number of stations need to be operated and, since they are manpower intensive, the data are fairly expensive (only 9 data values [u,v,h] over a six-hour period, assuming three-hour resolution). Overall a reasonable cost estimate would be \$15/datum.

2. Doppler Acoustic Sounder Systems, a relatively new development, also have the ability to provide station type data for u, v, and h. Observations can be continuous and can proceed while the equipment is unattended. Winds averaged over 0.5 hour should be within  $1 \text{ ms}^{-1}$  and inversion heights a few tens of metres, both quite adequate. The input format would be "mean layer vector wind and inversion base height by station location". The systems should develop reliability comparable to that for the monostatic systems as experience is gained. Data become available in real time but no spatial resolution is obtained. Simple monostatic sounder systems give inversion base height with equivalent advantages of operation. A network of monostatic sounders has been deployed in the Bay area for air quality purposes. Overall cost estimates are not available.
3. A meteorological aircraft can provide data over an extensive area of the domain with considerable flexibility of operation. Data collection can be in areas with difficult surface access, or in areas of particular concern for the specific episode. A typical aircraft will give a vector wind and temperature value every second, about every 100 m. With a well-designed flight pattern and real time data display it should be possible to obtain more than 20 independent

inversion height estimates and 50 mixed layer vector wind estimates over one hour of flight. Experience shows that considerable analysis is needed to obtain these values from the raw record. As the observation locations are variable, the appropriate data format is "mean layer vector wind and inversion base height by UTM location". Aircraft systems are less reliable than rawinsonde or minisonde systems, although reliability is improving. Because of the data rate cost per datum is relatively low, about \$8/datum based on \$500/hour aircraft cost.

An additional system which may have some potential in precipitation conditions, or where radar reflecting chaff can be deployed, is multiple Doppler radar. Currently there appears to be no experience with this system in Canada.

The least costly and most widely employed observing system is the surface observation. In application with MASCON LLL have made wide use of estimates of mean mixed layer vector wind derived from surface anemometer measurements. A power law wind profile is assumed so that

$$\bar{u}_h = u_{z_0} \int_{z_0}^h \left( \frac{z}{z_0} \right)^p dz$$

where  $z_0$  is anemometer height above the surface,  $u_{z_0}$  is wind speed at that height and  $p = 0.14$ . The mean mixed layer wind direction is assumed to be the same as the surface wind direction, an assumption which was found to be reasonable for the Bay area from a study of wind soundings (Dickerson, personal communication). No error estimates for this technique are available.

In the Bay area, which is well populated, existing surface anemometer stations are the prime meteorological data source for MASCON. This extensive data base does not exist in the AOSERP study area.

No formal studies appear to have been conducted to evaluate data requirements for MASCON. Results can be obtained given only a single wind and two inversion heights (to obtain  $\partial h/\partial t$ ) although this is not recommended. Subjectively the staff of LLL consider the results reasonable for the Bay area given the present observing network, 20 to 30 observations over a typical domain. Certainly judging by the pollution concentration predictions this would be the case, although the degree to which windfield errors would be noticed is not clear. A formal evaluation of data requirements would be in order before proceeding with application of the model, and would be costly only in computer resources.

#### 4.2.6 Computer Requirements

The task of implementing the MASCON code is, at least in concept, considerably more simple than that of implementing MATHEW or ADPIC. The code is written in standard FORTRAN IV, is well documented, and a user's manual is available. About one man-month of programmer time would be required for strict code conversion. Unfortunately such a code would operate at CMC only on a much reduced domain (for the same resolution), about 20 to 25% of the square 100 km on a side typically operated for the Bay area and encompassing the AOSERP area. There would be little point in operating this model on such a small area with so coarse a resolution.

Operating at LLL (and now Lawrence Berkley Laboratory), MASCON requires 53K SCM, 470K LCM and 1.5MW disk storage and executes an analysis in about 1 minute. Considering the smaller available SCM and LCM at CMC (Appendix 8.1), in order to operate MASCON on a full size grid there would require restructuring the code using overlays and using disk storage for working arrays. This restructuring effort would require at least three man-months of a skilled programmer-numerical analyst's time. Even so the code would likely execute considerably slower than LLL.

Additional programmer time would be required to rewrite the input and output routines to accommodate the remote batch operating system at CMC, and of course considerable programmer-meteorologist effort would be required in formulating case study input data.

#### 4.2.7 Evaluation

Advantages and disadvantages of MASCON are summarized in Table 8.

The only major problem in the model formulation is the conflict between the assumption  $dh/dt = 0$  used in deriving the layer-averaged continuity equation, and the estimation of  $(\partial h/\partial t) = (h_2 - h_1) (t_2 - t_1)$ . The extent and importance of this conflict needs further investigation.

From the point of view of model application to AOSERP problems one outstanding question is that of the validity of the mixed layer capped by inversion structure as being the predominant conditions of concern. The discussion in Section 2.3 indicates that it may indeed correspond to situations of concern in some instances.

Additional questions remain with respect to the costs on input data.

#### 4.3 LIRAQ-1

LIRAQ-1 is a computer model developed at LLL to simulate the physical processes applicable for non-chemically reactive pollutant species on the regional scale for the San Francisco Bay area. The model uses as input information on topography, meteorology (from MASCON), initial pollution concentrations, and source emissions, along with run data. The model simulates the temporal and spatial evolution of the pollutant concentrations. The physical processes concerned are horizontal and vertical advection (transport), horizontal

Table 8. Advantages and disadvantages of MASCON.

ADVANTAGES	DISADVANTAGES
Simpler and faster than MATHEW.	Applicable in more restrictive conditions than MATHEW
Attacks what is generally considered to be serious air quality condition-capping inversion.	Requires measurements of inversion heights which are difficult to obtain.
Allows mass leakage through the inversion lid.	Boundary condition $\lambda = 0$ implies $w_T \equiv 0$ at lateral boundary - potentially not consistent with topography at boundary.
Permits accounting of observed data with adjustments in least-squares sense	Interpolation of station observed winds to grid points by distance-weighting takes no account of topography
Several potential data source systems	Needs good observational data base
Considerable experience with application available at LLL	Resultant non-divergent flow is not necessarily accurate representation of actual flow
	Although resulting fields seem reasonable no formal verification or sensitivity studies published.
	$dh/dt=0$ not universally true $\alpha_1, \alpha_2$ should vary with stability

sub-grid scale eddy transport, deposition at the surface, simple species decay and pollutant source emissions. Model results are output in tabular, graphical, and computer compatible form.

The detailed description of LIRAQ-1 which follows is based on LLL contract reports (MacCracken 1975; MacCracken and Sauter 1975; and MacCracken et al. 1978) along with clarifying discussions with LLL personnel.

#### 4.3.1 Physical Basis

The conservation equation for pollutant species  $j$  is written in the summation convention notation

$$\frac{\partial c_j}{\partial t} + \frac{\partial}{\partial x_i} (u_i c_j) = \frac{\partial}{\partial x_i} \left( k_{x_i} \frac{\partial c_j}{\partial x_i} \right) + \frac{s_j}{\rho} + R_j$$

with the eddy diffusion parameterization for sub-grid scale transport terms. Here

$c_j$  is concentration (g/g) of pollutant species  $j$

$k_{x_i}$  are the eddy diffusion coefficients

$s_j$  is the non-chemical source and sink rate for pollutant species  $j$

$\rho$  is air density (assumed constant)

$R_j$  is in general the change in concentration due to chemical and photochemical species. For LIRAQ-1 this term is limited to representing only simple decay of species, independent of the concentration of any other species.

The model represents the atmospheric layer below an elevated inversion as a single layer. The conservation equation above is integrated from inversion height ( $H$ ) to the topographic surface (actually a reference level  $z_0$ , which is typically observation height). This is done by assuming functional forms for the wind and species concentration vertical profiles.

For the horizontal wind components the power-law profile

$$u_i(x, y, z, t) = u_{i_0}(x, y, z_0, t) \left( \frac{z}{z_0} \right)^n$$

is assumed. Integrating

$$\bar{u}_i = \frac{1}{H} \int_{z_0}^H u_i dz = \frac{u_{i_0}}{n+1} \left( \frac{H}{z_0} \right)^n = \frac{u_i H}{n+1}$$

A value  $n = 1/7$  is typically employed, best for neutral stratification.

For the concentration vertical profile a logarithmic form is assumed

$$c_j(x, y, z, t) = a_j(z, y, t) + b_j(z, y, t) \ln \left( \frac{z}{z_0} \right)$$

Integrating

$$\bar{c}_j = \frac{1}{H} \int_{z_0}^H c_j dz \approx a_j + b_j \left[ \ln \left( \frac{H}{z_0} \right) - 1 \right].$$

Similarly, for the product terms  $\bar{u}_i \bar{c}_j$  using the profile approximations and neglecting terms of order  $z_0/H$ .

$$\overline{u_i c_j} = \bar{u}_i \bar{c}_j \left[ 1 + \frac{b_j}{c_j} \frac{n}{n+1} \right]$$

The quantity  $\beta_j = b_j n / (c_j (n+1))$  is defined, so that  $\beta_j$  accounts for the effect of vertical non-uniformities in  $u_i$  and  $c_j$ . Typically  $\beta_j$  varies from -0.1 to 0.1.

The coefficients  $a_j$  and  $b_j$  are determined subject to two constraints. The first is derived from an analytical solution of the vertical turbulent diffusion equation for trace species applied to the thin layer from the surface to  $z_0$ . The assumption is made that the vertical pollutant distribution at  $z_0$  is in instantaneous

equilibrium and controlled only by vertical diffusion and surface sources and sinks. With the surface emission rate  $q_z$  and sink rate based on deposition velocity  $v_d$ .

$$K_z(x, y, z_0, t) \frac{\partial c_j}{\partial z} \Big|_{z=z_0} + \frac{q_j}{p} - v_d c_j(x, y, z_0, t) = 0$$

with fluxes considered positive into the layer below  $z_0$ .

The second constraint for determining  $a_j$  and  $b_j$  is the requirement that the vertical integral of concentration below the inversion be equivalent to the average value calculated using the integrated form of the species conservation equation

$$\bar{c}_j(x, y, t) = \frac{1}{H(x, y, t)} \int_0^{H(x, y, t)} c_j(x, y, z, t) dz.$$

Solving for  $a_j$  and  $b_j$

$$a_j = \frac{\left[ \frac{q_j}{p} \left( \frac{z_0}{H} - 1 + \ln \left( \frac{H}{z_0} \right) \right) + c_j \frac{K_{z_0}}{z_0} \right]}{\left[ \frac{K_{z_0}}{z_0} + v_d \left( \frac{z_0}{H} - 1 + \ln \left( \frac{H}{z_0} \right) \right) \right]}$$

$$\text{and } b_j = \left[ v_d \bar{c}_j - \frac{q_j}{p} \right] \left[ \frac{K_{z_0}}{z_0} + v_d \left( \frac{z_0}{H} - 1 + \ln \left( \frac{H}{z_0} \right) \right) \right]^{-1}$$

These forms allow a solution provided a non-zero minimum value of  $K_z$  is available. If there is neither deposition velocity nor a surface source,  $b_j = 0$  and there is a uniform vertical concentration profile given by  $c_j = a = \bar{c}_j$ . These terms provide for a surface concentration larger than the average if there are surface sources, and less than the vertical average if there is a surface deposition sink. Also, the weaker the vertical diffusion, the higher will be the surface concentration. With  $K_z$  a function of wind speed, this dependence causes higher surface concentrations in regions of weak winds, and lower concentrations in regions of strong winds. Maximum and minimum limits of the ratio of the surface concentration to the average concentration can also be imposed.

The integration of the conservation equation is done by multiplying through by the density of air (assumed constant) and integrating  $z_0$  to  $H$ . If, in general,  $f$  is some function of a variable  $q$  and:

$$\bar{f} = \frac{1}{H} \int_{z_0}^H f(z) dz ;$$

then:

$$\int_{z_0}^H \frac{\partial f}{\partial q} dz = \frac{\partial}{\partial q} (fH) - f(H) \frac{\partial H}{\partial q}$$

Applying this to the conservation equation,

$$\begin{aligned} & \frac{\partial}{\partial t} (\rho H \bar{c}_j) - \rho c_j(H) \frac{\partial H}{\partial t} + \frac{\partial}{\partial x} (\rho H \bar{u} c_j) - \rho c_j(H) u \frac{\partial H}{\partial x} + \frac{\partial}{\partial y} (\rho H \bar{v} c_j) \\ & - \rho c_j(H) v \frac{\partial H}{\partial y} + \rho w c_j \Big|_{z_0}^H = \frac{\partial}{\partial x} \left[ \rho H K_x \frac{\partial c_j}{\partial x} \right] - \rho K_x \frac{\partial c_j}{\partial x} \Big|_H \frac{\partial H}{\partial x} \\ & + \frac{\partial}{\partial y} \left[ \rho H K_y \frac{\partial c_j}{\partial y} \right] - \rho k_y \frac{\partial c_j}{\partial y} \Big|_H \frac{\partial H}{\partial y} + \rho k_z \frac{\partial c_j}{\partial z} \Big|_{z_0}^H + S_i + \rho H \bar{R}_j \bar{c}_j \end{aligned}$$

Defining  $\partial h/\partial t = w(H) - w_r$  where  $w_r$  is the vertical air velocity relative to the inversion at H. Define the flux:

$$w_j = -\rho c_j(H) \left[ \frac{\partial H}{\partial t} + u(H) \frac{\partial H}{\partial x} + v(H) \frac{\partial H}{\partial y} - w(H) \right] + \rho \left[ K_x \frac{\partial c_j}{\partial x} \Big|_H \frac{\partial H}{\partial x} + K_y \frac{\partial c_j}{\partial y} \Big|_H \frac{\partial H}{\partial y} - K_z \right]$$

representing the net effect of transport through the inversion. If  $\rho w_H$  is an effective air mass flux through the inversion, then there are three possible conditions corresponding to net flow into or out of the inversion and no net flow:

$$w_j = \begin{cases} \rho w_H c_j(x, y, H, t) & w_H > 0 \\ 0 & w_H = 0 \\ \rho w_H c_{Tj} & w_H < 0 \end{cases}$$

where  $c_j(x, y, H, t)$  is the concentration of species j at inversion base, and  $c_{Tj}$  is the background concentration of species j above the inversion.

For LIRAQ-1 the only remaining terms to be treated are the horizontal turbulent diffusion terms. The horizontal turbulent diffusion coefficient is often expressed in terms of the height dependent energy dissipation rate (Batchelor 1950). These diffusion terms are, however, small compared to the advection terms and the approximation  $K = K_x = K_y$  constant is reasonable. Applying this approximation leads to a final form for the vertically average conservation of species equation

$$\frac{\partial}{\partial t} (\bar{H}c_j) + \frac{\partial}{\partial x_i} \left[ \bar{H}c_j \bar{u}_i (1+\beta_j) \right] + \frac{w_j}{\rho} = \frac{\partial}{\partial x_i} \left[ K \frac{\partial}{\partial x_i} \bar{H}c_j \right] + \frac{s_j}{\rho} + \bar{H}R_j(c_j)$$

where the summation convention is applicable for subscript  $i$  for horizontal components only.

Finally in this section mention needs to be made of the treatment of elevated pollutant sources. This aspect is particularly important for AOSERP as the oil sands emissions are predominantly from elevated sources, as shown in Section 2.2. LIRAQ treats emission differently depending on the emission height. Source emissions below 30.1 m are assumed to affect the vertical concentration profile and form the surface source term. Emissions from more elevated sources are assumed to affect only the vertically averaged concentration. The effect is to assume a rapid vertical mixing of elevated source emissions which is not a serious problem in urban centres where surface sources dominate, but is highly unrealistic for the oil sands area when elevated sources predominate.

An additional feature of the treatment of elevated sources is the assumption of a distribution of source heights so that, depending on inversion height, elevated emissions are entirely within the mixed layer if the inversion is high, partially within it if the inversion is at intermediate height (100 to 150 m), but entirely above the inversion when the inversion is low. Nevertheless, when emissions are treated as above the mixed layer they are assumed not to affect the upper concentration boundary condition.

#### 4.3.2 Eddy Diffusivities

The vertical eddy diffusivity,  $K_z$ , is required only in determining the concentration profile coefficients  $a_j, b_j$ , and only at height  $z_0$  (near the surface). The constant stress layer expression for neutral stratification momentum diffusivity is assumed to hold,  $K_{z0} = k u_* z_0$ . Adopting the values  $k$  (von Karman's constant) = 0.4,  $u_* = 0.1 U_1$  with  $z_0 = 1$  m, obtain  $K_z = 0.04 U_1$ . The wind at height 1 m ( $U_1$ ) is obtained from the power law profile, with a minimum value  $0.1 \text{ ms}^{-1}$  specified. As a result the diffusivity varies to reflect wind speed variations, but there is no account of variations of surface roughness or stability.

Horizontal eddy diffusivity is derived empirically based on Bachelor's (1950) similarity theory (see MacCracken 1975)

$$K_H = 1.03 \times 10^{-2} U_1 \left[ H^{3/7} - 1 \right] \Delta s^{1/3}$$

with  $U_1$  the 1 m windspeed, H inversion base height and s the half-grid interval.

With the horizontal grid used in LIRAQ (1 km minimum, 5 km maximum), the explicit advection terms are normally substantially larger than the sub-grid diffusion terms. This is particularly the case for extended area sources. This being the case, the errors in the horizontal diffusion should not assume a great importance. Note again that because of spacial and temporal variations in  $U_1$  and H,  $K_H$  will reflect these variations. For pollution dominated by point sources, as for  $SO_2$  in the AOSERP study area, lateral horizontal eddy diffusion plays a critical role and the treatment in LIRAQ is quite suspect.

#### 4.3.3 Boundary Conditions

For each of the four horizontal and the top boundary a concentration exterior to the model domain is specified and used if there is inflow at the boundary involved. Outflow boundary concentrations are set to the values calculated at the outflow boundary.

The inflow-boundary concentrations are set by reference to background concentrations in the area of concern. For this reason it is important to eliminate the possibility of a major source upwind of a boundary--not currently a major problem for the oil sands area.

In certain circumstances the specification for concentration above the model top can become an important source of error. In the San Francisco Bay area it frequently occurs that there is locally considerable residual pollution from the previous day

above the top of the surface mixed layer. In addition substantial leakage through the inversion can occur locally, again tending to increase concentrations aloft. Where the inversion is low (>150 m) the prescription for elevated sources assumes emissions above the inversion. With each of these mechanisms the concentration aloft will be locally enhanced and downward entrainment as the inversion lifts will be mixing down significantly polluted air. Mainly because of a lack of knowledge about the variation of these concentrations aloft this remains an unresolved problem.

#### 4.3.4 Computational Formulation

LIRAQ-1 is applied on a finite difference grid, up to a maximum of 45 x 50 grid elements. Special attention is given to minimize errors arising because of the formulation. Details are in MacCracken et al. (1978) and MacCracken and Sauter (1975).

In solving the governing conservation of species equations the horizontal advection terms are treated first. A reformulated version of the Boris and Book (1973) flux-corrected transport (FCT) algorithm is applied as it minimizes the numerical diffusion problem often associated with finite difference formulations of these terms. FCT consists of two stages: an initial transport stage containing strong additional numerical diffusion; and a correction stage to remove, as far as possible, the numerical diffusion. The method is applied separately in the x and y directions with the order of application alternated for successive timestep. Readers are referred to the references for further details.

The treatment of the unresolved horizontal eddy fluxes follows the second-order prescription of MacCracken and Bornstein (1977). In essence the process is treated as an advective interchange of air mass between grid elements with both positive and negative velocities calculated by dividing the horizontal eddy diffusion coefficient ( $K_H$ ) by the grid length. Again the calculation is split in two-dimensions and the order of application alternated between time steps.

Next, vertical transport through the inversion is taken into account. This vertical transport is based on the flux required to accommodate mass-consistent winds and is calculated as the product of this mass flux and pollutant concentration at inversion base. Finally, effects of decay, deposition, and source emissions are computed.

#### 4.3.5 Data Requirements

To start up the model, concentrations of pollutant(s) are needed throughout the domain. Monitoring data, even in the well studied Bay area, are usually only available at a few points. The AOSERP area has, by comparison, a much greater deficiency of the area wide monitoring network. In addition, monitoring data are often not representative of the total grid area in which they are located owing to strong local concentration gradients. There are two answers to this problem: (1) Increase the monitoring coverage. The aircraft option discussed in Section 4.2.5 would be worth investigating here; and (2) Increase the period of time simulated so that concentrations of interest are at the end of the time period and not greatly influenced by initial concentrations.

Simulations for the Bay area have had to incorporate a highly complex emission inventory. This is because of the wide variety of sources in the region. By contrast, for the major emissions in the AOSERP area this will be less of a problem. The current emission inventory system should prove entirely adequate.

The above two data requirements have proven to be major problems for implementation of LIRAQ in urban areas. Another major problem, covered already in the discussion of MASCON, is data for the flow fields. Additional data requirements, such as for the parameterization of eddy diffusivity, deposition, etc., although required, tend to be less significant for the final concentration field.

#### 4.3.6 Computer Requirements

The LIRAW-1 model is written in the FORTRAN IV language and is well documented so that it can be compiled at CMC with only minimal effort. As with MASCON, however, the memory requirements are large. At LLL typically 47K SCM, 400K LCM and 2MW disk storage is employed in operating the model on a 45 x 50 grid element array. With two pollutants and a 24-hour simulation, the run time quoted is 55 minutes.

In order to restructure the code with overlays and use of disk storage for working arrays at least four man-months programmer-numerical analyst's time would be needed. Additional time would be required to restructure the problem formulator for the remote batch operating system. Realistically one would not expect to operate this model at CMC faster than about twice the speed of real time evolution.

#### 4.3.7 Evaluation

Advantages and disadvantages of LIRAQ-1 are summarized in Table 9. In addition the attributes of the MASCON driver model need to be considered (Section 4.2.7).

The formulation of the model as primarily suitable to treat extended pollutant sources and prohibitive run times makes LIRAQ-1 entirely unsuitable for AOSERP purposes.

#### 4.4 LIRAQ-2

The LIRAQ-2 models developed by LLL reflect the identical physical assumptions as are incorporated in LIRAQ-1 but with the addition of reactive pollutant species photochemistry. The information flow is very much as described for LIRAQ-1 and the general references given in Section 4.3 are applicable. LIRAQ-2, with the original chemistry, has been extensively applied in the San Francisco Bay area and, integrated with regional emission models, used to plan regional emissions control strategies (Hoffman et al. 1978).

Table 9. Advantages and disadvantages of LIRAQ-1.

ADVANTAGES	DISADVANTAGES
Minimizes artificial numerical diffusion	Not applicable for point sources
Treats an important meteorological condition for degraded air quality	No reactive chemistry
Allows for inversion leakage	Boundary and initial concentrations can be critical to solution, but may be difficult to define well.
Considerable experience with application at LLL	Assembly of input data is major undertaking.
	Prohibitively costly for computer execution times on current CMC system.

A more recent version of the model, LIRAQ-2S, incorporates a parameterization of atmospheric sulphur chemistry in addition to photochemical oxidation processes. Application of this version of the model is discussed by Duewer et al. (1978).

#### 4.4.1 Model Chemistry

The LIRAQ photochemical submodels are designed to reproduce homogeneous inorganic chemistry with the best available measurements or estimates for reaction-rate constants. The organic species are approximated using a 'lumping' scheme whereby classes of compounds reacting with the same set of species are grouped together. Finally, consistent with the discussion of lifetimes given in Appendix 8.2, certain inorganic species are represented as in photochemical equilibrium.

In the more recent LIRAQ-2S a simple homogeneous scheme for sulphur chemistry is included.

The reaction set used in the LIRAQ-2 contains 16 inorganic species for which differential equations must be solved in each grid element. Some economy in computation is attained by holding certain species in steady-state where they may be considered 'inert' and well mixed, or in photochemical equilibrium. The reactions are given in Table 10. The Arrhenius expression used for the reaction rate is  $K = A \exp(-C/T)$ .

An explicit mechanistic model incorporating all organic species is totally impracticable. More than 200 distinct chemical species have been identified in gasoline and exhaust gases, solvents, etc. may increase that inventory substantially. The reactions involving organics are most inadequately understood particularly those between organic-free radicals, moreover rate data are almost totally absent. This lack of reliable mechanistic data is particularly acute for atmospheric conditions where unstable collision complexes may be stabilized or react with ambient oxygen to produce products not observable in the low pressure and inert atmosphere experiments for which laboratory data are available.

Table 10. Reaction set used in LIRAQ-2.

Reactions	Arrhenius Parameters		
	A,	cm s <sup>-1</sup>	C
NO <sub>2</sub> + hν = NO + O			
O + O <sub>2</sub> + M = O <sub>3</sub> + M	1.07	E-34	-510.
O <sub>3</sub> + NO = NO <sub>2</sub> + O <sub>2</sub>	9.0	E-13	1200.
O + NO + M = NO <sub>2</sub> + M	4.0	E-33	-940.
O + NO <sub>2</sub> = NO + O <sub>2</sub>	9.1	E-12	
O + NO <sub>2</sub> + M = NO <sub>3</sub> + M	3.5	E-32	-300.
O <sub>3</sub> + NO <sub>2</sub> = NO <sub>3</sub> + O <sub>2</sub>	1.10	E-13	2450.
NO <sub>3</sub> + NO <sub>2</sub> = N <sub>2</sub> O <sub>5</sub>	3.80	E-12	
N <sub>2</sub> O <sub>5</sub> = NO <sub>2</sub> + NO <sub>3</sub>	5.7	E+14	10600.
NO <sub>3</sub> + NO = 2NO <sub>2</sub>	8.7	E-12	
N <sub>2</sub> O <sub>5</sub> + H <sub>2</sub> O = 2HNO <sub>3</sub>	3.0	E-16	3300.
HNO <sub>2</sub> + hν = HO + NO			
HO + NO <sub>2</sub> = HNO <sub>3</sub>	5.0	E-12	
HO + NO = HNO <sub>2</sub>	5.0	E-12	
HO + CO = CO <sub>2</sub> + HO <sub>2</sub>	1.40	E-13	
HO <sub>2</sub> + NO = HO + NO <sub>2</sub>	3.0	E-12	700.
H <sub>2</sub> O <sub>2</sub> + hν = 2HO			
HCl + O = RO <sub>2</sub> + RCO <sub>3</sub> + (1-α)HO <sub>2</sub>	1.0	E-11	360.
HCl + O <sub>3</sub> = HO <sub>2</sub> + RO + HC4	7.0	E-15	1900.
HCl + HO = RO <sub>2</sub> + HC4	5.0	E-11	350.
HC2 + O = RO <sub>2</sub> + HO	4.1	E-11	2000.
HC2 + HO = RO <sub>2</sub> + H <sub>2</sub> O	4.0	E-11	900.
HC4 + hν = RO <sub>2</sub> + HO <sub>2</sub>			
HC4 + HO = RCO <sub>3</sub> + H <sub>2</sub> O	3.0	E-11	350.

Continued ...

Table 10. Concluded.

Reactions	Arrhenius Parameters		
	A, cm s <sup>-1</sup>		C
RO <sub>2</sub> + NO = RO + NO <sub>2</sub>	3.3	E-12	300.
RCO <sub>3</sub> + NO = RO <sub>2</sub> + NO <sub>2</sub> + CO <sub>2</sub>	6.5	E-12	600.
RCO <sub>3</sub> + NO <sub>2</sub> = PAN	2.95	E-14	
RO + O <sub>2</sub> = HO <sub>2</sub> + HC4	1.6	E-13	3300.
RO + NO <sub>2</sub> = RNO <sub>3</sub>	5.0	E-14	
RO + NO = RNO <sub>2</sub>	5.0	E-14	
HO <sub>2</sub> + HO <sub>2</sub> = H <sub>2</sub> O <sub>2</sub> + O <sub>2</sub>	3.0	E-11	500.
RO <sub>2</sub> + HO <sub>2</sub> = RO + HO + O <sub>2</sub>	6.7	E-14	
RO <sub>2</sub> + RO <sub>2</sub> = 2RO + O <sub>2</sub>	6.7	E-14	
HC4 + O = HO + HO <sub>2</sub> + CO	4.0	E-12	900.
RNO <sub>2</sub> + hν = RO + NO			
HC4 + hν = 2HO <sub>2</sub> + CO			
NO <sub>3</sub> + hν = NO <sub>2</sub> + O			
HO <sub>2</sub> + HC4 = H <sub>2</sub> O <sub>2</sub> + RCO <sub>3</sub>	8.0	E-13	3700.
RO <sub>2</sub> + HC4 = ROOH + RCO <sub>3</sub>	8.0	E-13	3750.
O <sub>3</sub> + hν = O + O <sub>2</sub>			
O <sub>3</sub> + hν = <sup>H<sub>2</sub>O</sup> O <sub>2</sub> + 2HO			
HO <sub>2</sub> + NO <sub>2</sub> = HNO <sub>2</sub> + O <sub>2</sub>	1.0	E-12	1200.
NO <sub>3</sub> + HC4 = RCO <sub>3</sub> + HNO <sub>3</sub>	3.0	E-15	900.
HO + HO <sub>2</sub> = H <sub>2</sub> O + O <sub>2</sub>	2.0	E-10	
HC4 + HO = CO + HO <sub>2</sub> + H <sub>2</sub> O	3.0	E-11	350.
NO <sub>3</sub> + HC4 = CO + HNO <sub>3</sub> + HO <sub>2</sub>	3.0	E-15	650.
HCl + HO = RO <sub>2</sub> + H <sub>2</sub> O	3.0	E-11	350.
HO + HNO <sub>3</sub> = H <sub>2</sub> O + NO <sub>3</sub>	9.0	E-14	

In light of the foregoing constraints, LLL scientists adopted the method of grouping the hydrocarbons into three classes in terms of their tendencies to react with the same set of species. The classes chosen were:

1. HC-1 - hydrocarbons reacting with O, O<sub>2</sub>, and OH; generally speaking, alkenes and reactive aromatic compounds.
2. HC-2 - hydrocarbons reacting with O and OH; i.e., alkanes, some ketones, less reactive aromatic compounds, many alkyl halides etc.; and
3. HC-4 - hydrocarbons in this class are photolyzed and react with OH and O, and slowly with peroxy radicals and NO<sub>3</sub>; i.e., aldehydes, some aromatic compounds, some ketones, etc.

The classes of products from these simulations of hydrocarbon reactions are symbolized as follows:

1. RO - alkoxy radicals;
2. RO<sub>2</sub> - alkyl peroxy radicals;
3. RCO<sub>3</sub> - peroxy acyl radicals;
4. ROOH - organic hydroperoxide;
5. RNO<sub>2</sub> - organic nitrite;
6. RNO<sub>3</sub> - organic nitrate; and
7. PAN - peroxyacyl nitrate.

The lumping of many similar species into one average species results in a set of pseudo-rate coefficients that only approximately describe the reactions of the individual compounds in the class. These 'coefficients' are in fact parameters that must be 'tuned'. If there is a wide range of rates for individual members of a class and relative concentrations vary, pseudo-rate coefficient of the class could vary with time.

In practice to develop rate constants for each class they were treated as follows:

1. HC-1 - as propane, effective molecular weight 44;
2. HC-2 - as n-butane, effective molecular weight 58; and
3. HC-4 - as equimolar mixture of formaldehyde and acetaldehyde, effective molecular weight 38.

Measured values are generally reported as total hydrocarbon including methane. The background methane ( $\sim 1.5$  ppm) which has a very low reactivity even relative to other HC-2 class species was excluded in carrying out photochemical computations.

The sulphur chemistry treated in LIRAQ-2S neglects the contribution of heterogeneous phase-reactions involving dissolution of  $\text{SO}_2$  and  $\text{O}_2$  in water droplets followed by metal ion catalyzed oxidation in favour of the homogeneous gas phase oxidation now considered to be more important. The reaction set is shown in Table 11.

#### 4.4.2 Computational Formulation

With the treatment of a large number of chemical species, the demand for computer storage in LIRAQ-2 is considerably increased over that for LIRAQ-1. This is accommodated at the cost of decreasing the number of grid points. A more challenging difficulty is that more equations need to be solved and these have a wide range of associated characteristic time scales. To meet these new demands the treatment of the terms in the governing equation representing vertical advection through the inversion, horizontal eddy mixing, pollutant source, decay and deposition to the surface, need not be changed from LIRAQ-1.

The method of Gear (1971), a high order iterative-extrapolation procedure, is used to advance the concentration field in time. Because of this formulation the FCT algorithm cannot be applied to the horizontal advection terms as in LIRAQ-1. Instead a simple upstream difference technique after Molenkamp (1968) is used. Duewer et al. (1978) show that, despite the frequently quoted theoretical deficiencies of upstream differencing, LIRAQ-1 and LIRAQ-2 compare quite well.

An additional simplification in LIRAQ-2 which eases the computational load is the neglect of the B terms in the governing equations. The effect of this is to ignore the implication of any vertical inhomogeneity in the species concentration profiles on overall reaction rates and horizontal advections.

Table 11. Reaction set used in LIRAQ-2S.

Reaction	Arrhenius parameters		
	A, cm s <sup>-1</sup>	C, K	
Photolysis			
$O_3 + h\nu = O + O_2$			
$O_3 + h\nu \xrightarrow{H_2O} O_2 + 2OH$			
$NO_2 + h\nu = NO + O$			
$NO_3 + h\nu = NO_2 + O$			
$HNO_2 + h\nu = HO + NO$			
$H_2O_2 + h\nu = 2OH$			
$HC_4 + h\nu = RCO_3 + HO_2$			
$HC_4 + h\nu = CO$			
$O_x$ - $NO_x$ - $HO_x$ Reactions			
$O + O_2 + M = O_3 + M$	1.07	E-34	510
$O_3 + NO = O_2 + NO_2$	1	E-12	-1200
$O + NO + M = NO_2 + M$	4.0	E-33	940
$O + NO_2 = NO + O_2$	9.1	E-12	0
$O + NO_2 + M = NO_3 + M$	3.5	E-32	300
$O_3 + NO_2 = NO_3 + O_2$	1.1	E-13	-2450
$NO_2 + NO_3 = N_2O_5$	3.8	E-12	0
$N_2O_5 = NO_2 + NO_3$	5.7	E+14	-10600
$NO + NO_3 = 2NO_2$	8.7	E-12	0
$N_2O_5 + H_2O = 2HNO_3$	3.0	E-16	-3300
$HO + NO_2 = HNO_3$	1.0	E-11	0
$HO + NO = HNO_2$	6.0	E-12	0
$HO + CO = CO_2 + HO_2$	1.4	E-13	0

Continued ...

Table 11. Continued.

Reaction	Arrhenius parameters		
	A, cm s <sup>-1</sup>		C, K
HO <sub>2</sub> + NO = HO + NO <sub>2</sub>	1	E-11	-350
HO + HO <sub>2</sub> = H <sub>2</sub> O + O <sub>2</sub>	2	E-11	0
HO <sub>2</sub> + 2NO <sub>2</sub> = HNO <sub>2</sub>	2	E-14	0
HO <sub>2</sub> + O <sub>3</sub> = HO + 2O <sub>2</sub>	6.0	E-14	-1220
HO + O <sub>3</sub> = HO <sub>2</sub> + O <sub>2</sub>	1.6	E-12	-1000
HO + HNO <sub>3</sub> = H <sub>2</sub> O + NO <sub>3</sub>	9	E-14	0
HO <sub>2</sub> + HO <sub>2</sub> = H <sub>2</sub> O <sub>2</sub> + O <sub>2</sub>	1.7	E-11	-500
Reactions of HC <sub>1</sub>			
HC <sub>1</sub> + O = RO <sub>2</sub> + RCO <sub>3</sub>	1	E-11	-360
HC <sub>1</sub> + O <sub>3</sub> = HO <sub>2</sub> + RO + HC <sub>4</sub>	7	E-15	-1900
HC <sub>1</sub> + HO = RO <sub>2</sub> + HC <sub>4</sub>	4	E-11	-120
HC <sub>1</sub> + HO = RO <sub>2</sub> + H <sub>2</sub> O	3	E-11	-350
HC <sub>1</sub> + NO <sub>3</sub> = NO <sub>2</sub> + H <sub>2</sub> O	5	E-13	-1400
HC <sub>1</sub> + HO <sub>2</sub> = HO + HC <sub>2</sub>	0		0
Reactions of HC <sub>2</sub>			
HC <sub>2</sub> + O = RO <sub>2</sub> + HO	3.2	E-11	-2000
HC <sub>2</sub> + HO = RO <sub>2</sub> + H <sub>2</sub> O	4.5	E-11	-900
Reactions of HC <sub>4</sub>			
HC <sub>4</sub> + HO = RCO <sub>3</sub> + H <sub>2</sub> O	1.5	E-11	-350
HC <sub>4</sub> + O = HO + RCO <sub>3</sub>	3.2	E-12	-900
HC <sub>4</sub> + HO <sub>2</sub> = H <sub>2</sub> O <sub>2</sub> + RCO <sub>3</sub>	8	E-13	-3700
HC <sub>4</sub> + HO = CO + HO <sub>2</sub> + H <sub>2</sub> O	3	E-11	-350

Continued ...

Table 11. Concluded.

Reaction	Arrhenius parameters		
	A, cm s <sup>-1</sup>		C, K
$\text{HC}_4 + \text{NO}_3 = \text{RCO}_3 + \text{HNO}_3$	3	E-15	-900
$\text{HC}_4 + \text{RO}_2 = \text{ROOH} + \text{RCO}_3$	8	E-13	-3750
Reactions of SO <sub>2</sub>			
$\text{HO}_2 + \text{SO}_2 = \text{HO} + \text{SO}_4^-$	9	E-16	0
$\text{HO} + \text{SO}_2 = \text{HO}_2 + \text{SO}_4^-$	6	E-13	0
$\text{RO} + \text{SO}_2 = \text{HO}_2 + \text{SO}_4^-$	4	E-13	0
$\text{RO}_2 + \text{SO}_2 = \text{RO} + \text{SO}_4^-$	2	E-15	0
$\text{RCO}_3 + \text{SO}_2 = \text{RO}_2 + \text{SO}_4^- + \text{CO}_2$	1	E-15	0
Organic Radical Reactions			
$\text{RCO}_3 + \text{RCO}_3 = \text{HC}_4 + \text{CO}_2$	1	E-12	0
$\text{RO}_2 + \text{NO} = \text{RO} + \text{NO}_2$	4	E-12	-300
$\text{RCO}_3 + \text{NO} = \text{RO}_2 + \text{NO}_2 + \text{CO}_2$	3	E-12	-300
$\text{RCO}_3 + \text{NO}_2 = \text{PAN}$	2.7	E-13	0
$\text{RO} + \text{O}_2 = \text{HO}_2 + \text{HC}_4$	1	E-12	-2200
$\text{RO} + \text{NO}_2 = \text{RNO}_3$	2	E-12	0
$\text{RO} + \text{NO} = \text{RNO}_2$	2	E-12	0
$\text{RO}_2 + \text{HO}_2 = \text{ROOH} + \text{O}_2$	2.7	E-12	0
$\text{RO}_2 + \text{RO}_2 = \text{RO} + \text{RO} + \text{O}_2$	2.7	E-13	0

#### 4.4.3 Data Requirements

In addition to the data requirements described for MASCON and LIRAQ-1, concentration of each species is needed initially across the model domain.

In the Bay area measurements of CO, NO, NO<sub>2</sub>, SO<sub>2</sub>, and O<sub>3</sub> are available and are accepted at face value. The concentrations in the hydrocarbon classes HC-1, HC-2, and HC-4 are generated from measurements of total hydrocarbons (THC) and of methane. From these initial surface station concentrations, mixing depth, wind speed and emissions, a mean layer concentration is calculated. Mean layer concentrations are then interpolated to the grid using a Gaussian interpolation scheme. Portions of the domain where the topography is above the mixing depth are assigned concentrations of the upper boundary. This method of generating initial conditions for stable species is questionable for regions of complex terrain and source patterns particularly where initialization from sparse data is unavoidable.

The initial conditions for H<sub>2</sub>O<sub>2</sub>, HNO<sub>2</sub>, HNO<sub>3</sub>, and SO<sub>4</sub> are set equal to the assumed background levels. Predictions for most species are insensitive to the choice of HNO<sub>3</sub> and SO<sub>4</sub> but that is not so for H<sub>2</sub>O<sub>2</sub> and HNO<sub>2</sub>. The values chosen,  $4 \cdot 10^{-4}$  ppm, are somewhat poorly justified and could well affect the predicted species concentrations. For those species treated as in steady-state the values were derived by iterative solution of the relevant algebraic equations.

The emissions inventory currently included in LIRAQ-2 is representative of the San Francisco Bay area and determined from an extensive observational program. Even in the Bay area hydrocarbon data are only available as total hydrocarbons and the fractionation of this into the three hydrocarbon classes (HC-1, HC-2, and HC-4) may not be appropriate to any other location and source distribution. LIRAQ, moreover, requires emissions hourly and where less time resolution is available one must assume some time variation that will depend on a knowledge of the sources concerned.

#### 4.4.4 Computer Requirements

Although the number of grid elements used in LIRAQ-2 is smaller than for LIRAQ-1, 20 x 20 compared to 45 x 50, the memory requirements are quite similar because many more variables need to be specified at each grid point. LIRAQ-2 executes in about 60 minutes for a 24-hour simulation, marginally slower than LIRAQ-1.

The code conversion problems are the same as for LIRAQ-1, arising because of limited core capacity at CMC. Thus a similar slowdown in computer execution time, about a factor ten, could be expected making application impractical with the present facilities.

#### 4.4.5 Evaluation

Advantages and disadvantages of LIRAQ-2 and LIRAQ-2S are summarized in Table 12. Again the model is inappropriate for the AOSERP problem, being a point source problem rather than an extended source one. Further, the model is impractical with the current Canadian computer resources.

Table 12. Advantages and disadvantages of LIRAQ-2.

ADVANTAGES	DISADVANTAGES
Provides an integrated treatment of major atmospheric processes effecting pollutant concentrations	Not applicable for the AOSERP elevated point source problem
Considerable experience with application at LLL	Does not incorporate heterogeneous chemistry or wet deposition
Results have proven realistic and useful in Bay area episode pollution studies	Current pollution monitoring in the AOSERP area is inadequate for model initialization
	Current Canadian computer facilities inadequate for this model

5.

CONCLUSIONS

1. The difficulty of finding an "off the shelf" model for application to the Alberta Oil Sands area became apparent during this study. Even the two models identified by Padro (1977) as having potential application are found to have several practical difficulties.
2. Under the auspices of AOSERP, considerable progress has been made in understanding pollution processes in the oil sands region. Much remains to be done. A significant lack from the modelling viewpoint is that meteorological conditions of concern for environmental impact (episode situations) are not yet well defined. It does appear that, at least for certain episode conditions, the Gaussian approach is inadequate.
3. The ADPIC-MATHEW air quality assessment package offers considerable potential in the long term because of its generality. There are, however, several limitations imposed by inadequate physics (e.g., the diffusion parameters) and by the mathematical technique (e.g., the specification of the Gauss precision moduli). Another limitation is that the model has not yet been implemented for reactive atmospheric pollutant species (i.e., the photochemical oxidant problem). The generality of the package demands a large computer resource, apparently beyond the scope of current Canadian availability.
4. The LIRAQ models have proven their utility for urban air quality assessment in the San Francisco Bay area. The dominance of point source emissions in the oil sands area, which the LIRAQ models do not handle well, means that these models have only marginal utility for AOSERP. The LIRAQ mixed layer formulation may also be an unacceptably restrictive

assumption. In addition requirements for computer resources appear to be beyond current Canadian availability.

5. Of the models reviewed, the PATRIC code offers the most practicable potential for AOSERP studies. Attention needs to be given to certain problems and limitations of the current formulation for AOSERP implementation. Although the model has been used for long-term assessment studies by LLL workers, computer limitations in Canada will require extensive model reprogramming and likely restrict current application to episode conditions.

6. RECOMMENDATIONS

1. As a matter of priority it is recommended that AOSERP investigate the requirement for episode-type studies appropriate for complex non-Gaussian models on the scale in question.
2. If such episode studies are found to be important, then it is recommended that studies be continued to bring into focus those meteorological conditions of most concern for environmental impact in the oil sands area. For each condition identified, archetypes of the three-dimensional wind and stability fields, and their evolution as necessary, need to be established. It is important that these be specified without consideration of model limitations.
3. It is recommended that information and definition of episode conditions be refined by additional special model-directed intensive observations. Serious consideration needs to be given to the advantages of data acquisition by a meteorological aircraft system sensing mean wind and other state parameters.
4. Continuation of AOSERP studies of physical processes occurring in the atmosphere is recommended. Additional emphasis needs to be placed on simplification of parameterizations.

7. REFERENCES CITED

- Barrie, L.A., 1978. The concentration and deposition of sulphur compounds and metals around the GCOS oil extraction plant during June, 1977. Prep. for the Alberta Oil Sands Environmental Research Program, Edmonton. Project Me 1.5.3.
- Barrie, L.A., V. Nespliak, and J. Arnold. 1978. Chemistry of rain in the Athabasca oil sands region: summer 1977. Atmospheric Environment Service. Internal Report ARQT 3-78. 70 pp.
- Barrie, L.A., and J.L. Walmsley. 1978. A study of sulphur dioxide deposition velocities to snow in northern Canada. Atmospheric Environment 12:2321-2332.
- Boris, J., and D.L. Book. 1973. Flux corrected transport. I. SHASTA, A fluid transport algorithm that works. J. Comput. Phys. 11:38-69.
- Bottenheim, J.W., and G.P. Strausz. 1977. Review of pollutant transformation processes relevant to the Alberta oil sands area. Prep. for the Alberta Oil Sands Environmental Research Program, Edmonton. AOSERP Report 25. 166 pp.
- Businger, J.A., J.C. Wyngaard, Y. Izumi, and E.F. Bradley. 1971. Flux-profile relationships in the atmospheric surface layer. J. Atmos. Sci. 28:181-189.
- Dickerson, M.H. 1978. MASCON - A mass consistent atmospheric flux model for regions with complex terrain. J. Appl. Meteor. 17:241-253.
- Duewer, W.H., J.J. Walton, K.E. Grant, and H. Walker. 1978. Livermore regional air quality (LIRAQ) application to St. Louis, Missouri. Lawrence Livermore Laboratory Report. UCRL-52432. 81 pp.
- Finlayson, B.A. 1972. The method of weighted residuals and variational principles academic press. 412 pp.
- Forsythe, G.E., and W.R. Wasow. 1960. Finite difference methods for partial differential equations. Wiley. 444 pp.
- Gear, C.W. 1971. The automatic integration of ordinary differential equations. Comm. A.C.M. 14(3):176-179.
- Haltiner, G.J., and F.L. Martin. 1957. Dynamical and physical meteorology. McGraw-Hill. 470 pp.

- Hildebrand, F.B. 1962. Advanced calculus for application. Prentice-Hall. 646 pp.
- Hoffman, S.R., E.Y. Leong, and R.Y. Wada. 1978. Air quality plan development in the San Francisco Bay region: integrating complex regional models into the decision making process. Presented at the American Institute of Planners 61st Annual Conf. New Orleans.
- Lange, R. 1978<sup>a</sup>. ADPIC - a three-dimensional particle-in-cell model for the dispersal of atmospheric pollutants and its comparison to regional tracer studies. J. Appl. Meteor. 17:320-329.
- Lange, R. 1978<sup>b</sup>. PATRIC, a three-dimensional particle-in-cell sequential puff code for modelling the transport and diffusion of atmospheric pollutants. Lawrence Livermore Laboratory Report UCID-17701. 8 pp.
- Lusis, M.A., K.G. Anlauf, L.A. Barrie, and H.A. Wiebe. 1978. Plume chemistry studies at a northern Alberta power plant. Atmospheric Environment. 12:2429-2437.
- MacCracken, M.C. 1975. User's guide to the LIRAQ model: an air pollution model for the San Francisco Bay area. Lawrence Livermore Laboratory Report. UCRL-51983.
- MacCracken, M.C., and R.D. Bornstein. 1977. On the treatment of advection in flux formulations for variable grid models, with application to two models of the atmosphere. J. Comput. Phys. 23:135-149.
- MacCracken, M.C., and G.D. Sauter, eds. 1975. Development of an air pollution model for the San Francisco Bay area, final report, Volumes I and II. Lawrence Livermore Laboratory Report. UCRL-51920.
- MacCracken, M.C., D.J. Wuebbles, J.J. Walton, W.H. Duewer, and K.E. Grant. 1978. The Livermore regional air quality model: 1. Concept and development. J. Appl. Meteor. 17:254-272.
- Molenkamp, C.R. 1968. Accuracy of finite-difference methods applied to the advection equation. J. Appl. Meteor. 7:160-167.
- Padro, J. 1977. Review of dispersion models - possible applications in the Alberta oil sands. Prep. for the Alberta Oil Sands Environmental Research Program, Edmonton. Project ME 4.2.1.
- Pendergast, M.M. 1976. Estimating diffusion coefficients from meteorological data. DP-MS-76-64. Savannah River Laboratory, E.I. du Pont de Nemours & Co.

- Shelfentook, W. 1978. An inventory system for atmospheric emissions in the AOSERP study area. Prep. for the Alberta Oil Sands Environmental Research Program, Edmonton. AOSERP Report 29. 58 pp.
- Sherman, C.A. 1978. A mass-consistent model for wind fields over complex terrain. J. Appl. Meteor. 17:312-319.
- Stroscher, M.M. 1978. Ambient air quality in the AOSERP study area, 1977. Prep. for the Alberta Oil Sands Environmental Research Program, Edmonton. AOSERP Report 30. 74 pp.
- Walmsley, J.L., and D.L. Bagg. 1977. Calculatons of annual average sulphur dioxide concentrations at ground level in the AOSERP study area. Prep. for the Alberta Oil Sands Environmental Research Program, Edmonton. AOSERP Report 19. 40 pp.
- Whelpdale, D.M., and R.W. Shaw. 1974. Sulphur dioxide removal by turbulent transfer over grass, snow and water surfaces. Tellus. 26:196-205.

8. APPENDICES

## 8.1 COMPARATIVE COMPUTER RESOURCES AT LLL AND AT CMC

Significant differences exist between the computer system used to run the air quality systems at LLL and the CMC computer system. LLL and CMC 7600 computers can be compared as follows:

<u>System</u>	<u>SCM</u>	<u>LCM</u>	<u>O/S</u>	<u>Performance</u>
LLL	65 KW	512 KW	TS	1.5
CMC	32 KW	256 KW	RB	1.0

The LLL system has twice the memory of the CMC system and runs a time sharing (TS) operating system as opposed to the CMC remote batch (RB) operating system. This means that, in terms of overall processing capability, the LLL system can carry 50% more load than the CMC system.

The operating systems in use on the 7600's affect the amounts of memory available to user programs. The user available memory of the LLL and CMC systems can be compared as follows:

<u>System</u>	<u>SCM</u>	<u>LCM</u>
LLL	57 KW	490 KW
CMC	24 KW	125 KW

As can be seen, programmers at LLL have much more available memory than available at CMC.

A final factor affecting machine performance on the 7600 type of computer is the type of disk system used for system mass storage. The disk system characteristics can be discussed in terms of capacity, access time and transfer rate from disk to memory. For the purposes of the LLL air quality models, both CMC and LLL have more than adequate available on line disk storage. Disk access time is not highly variable between the various types of disk that can be used on the 7600; however, the nature of the physical disk sub-system can affect the performance of the disks by a factor of 2 or more. All LLL disks are dual access configuration type 817 or type 819 disks. At CMC the disk system is single access type 819 or type

844. The MASCON/LIRAQ system is implemented for operation use on the Lawrence Berkley Laboratory 7600 system (LBL) using 817 type disks so that quoted machine times for this model incorporate a factor for disk access that has double the possible CMC performance.

The transfer rates of the various disk types are as follows:

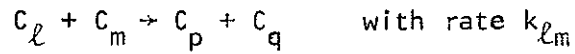
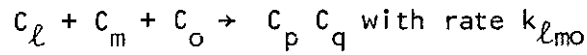
Type	844	817	819
Rate Ratio	1.0	6.0	4.0

The transfer rate has a strong influence on operating system performance in terms of job throughput, and a drastic affect on the time required to execute an input-output bound program. As implemented on the LLL and LBL computer systems, the air quality models are not input/output bound models. They make use of the available memory to hold all the required data in memory, using the disks for input data files and output of results. If these models were to be implemented at CMC, they would require the use of disks for intermediate working storage, thus boosting the required machine time for program execution by a factor of about 10.

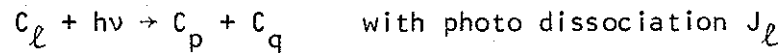
## 8.2 CHEMICAL KINETIC CONCEPTS

Most constituents of the atmosphere, whether naturally occurring or attributable to man's activities, interact chemically with one another. The simplest scheme of atmospheric reactions is that occurring between gaseous constituents (homogeneous reactions) though the effects of the presence of liquid and solid aerosol particles in suspension may be allowed for by heterogeneous or mixed-phase reactions in which the elementary steps involve particle-sticking coefficients and catalytic activity. Neither LIRAQ-2, which deals with photochemical smog chemistry, nor LIRAQ-2S, which includes in addition SO<sub>2</sub> and sulphate modelling capabilities, explicitly includes mixed-phase reactions.

Within a unit mass of atmosphere containing  $Z$  gaseous chemical species a complete reaction scheme may be represented by a set of  $S$  reactions of three types:



and



$n$  represents the number density of the constituent identified by the subscript  $\ell, m, n, o, p, q$  between 1 and  $Z$ .  $J_\ell$  varies with solar zenith angle (latitude, time of day and date) and the reaction rates  $k_{\ell mo}$  and  $k_{\ell m}$  may be temperature dependent.

The net rate of change of constituent  $C_p$  attributable to chemical reactions is

$$\frac{\partial C_p}{\partial t} = P_p - Q_p C_p - R_p C_p^2 \quad (B1)$$

where  $P_p$ ,  $Q_p$ , and  $R_p$  are functions of type:

$$P_p = \sum J_\ell C_\ell + \sum k_{\ell mo} C_\ell C_m C_o + \sum k_{\ell m} C_\ell C_m, \quad p \neq \ell, m, o$$

$$Q_p = \sum J_\ell + \sum k_{\ell mp} C_\ell C_m + \sum k_{\ell p} C_\ell$$

$$R_p = \sum k_{\ell pp} C_\ell + \sum k_{pp}$$

If  $R \equiv 0$  and  $Q$  is constant a solution to the rate equation (B1) would take the form:  $(C - C_\ell) = (C_i - C_\ell) \exp(-Qt)$  where  $C_i$  is the value of  $C$  at  $t = 0$ , and  $C$  is the photo-chemical equilibrium value as  $t \rightarrow \infty$  and is equal to  $P/Q$ . We can thus define a lifetime for that constituent as the time necessary for the departure of photo-chemical equilibrium to drop to  $\exp(-1)$  of its initial value, i.e.  $(C - C_\ell)/(C_i - C_\ell) = \exp(-1)$ ,  $\tau = 1/Q$ .

In general  $Q_p$  varies with height, time of day and season since it is a function of time-varying rates of photo-dissociation, temperature-dependent reaction rates, and constituent concentrations that are modulated by transport processes and chemical reactions. Assuming, however, that  $Q_p$  is considered uniform throughout the region

under consideration, the relative importance of chemical transformations can be roughly assessed. Since the LIRAQ-2 and LIRAQ-2S models are used to predict pollutant distributions for about a day duration with time steps of a fraction of an hour, any constituent,  $C_p$ , for which  $\tau = 1/Q_p$  is of the order of seconds or less may be considered to be in photochemical equilibrium ( $C_p = C_p = P_p/Q_p$ ).

In the LIRAQ-2 model these general concepts are applied under the restrictive constraints imposed by computer limitations, lack of knowledge about the nature and rates of many individual reactions, and the difficulty of specifying the source emissions in the model.

9. AOSERP RESEARCH REPORTS

1. AOSERP First Annual Report, 1975
2. AF 4.1.1 Walleye and Goldeye Fisheries Investigations in the Peace-Athabasca Delta--1975
3. HE 1.1.1 Structure of a Traditional Baseline Data System
4. VE 2.2 A Preliminary Vegetation Survey of the Alberta Oil Sands Environmental Research Program Study Area
5. HY 3.1 The Evaluation of Wastewaters from an Oil Sand Extraction Plant
6. Housing for the North--The Stackwall System
7. AF 3.1.1 A Synopsis of the Physical and Biological Limnology and Fisheries Programs within the Alberta Oil Sands Area
8. AF 1.2.1 The Impact of Saline Waters upon Freshwater Biota (A Literature Review and Bibliography)
9. ME 3.3 Preliminary Investigations into the Magnitude of Fog Occurrence and Associated Problems in the Oil Sands Area
10. HE 2.1 Development of a Research Design Related to Archaeological Studies in the Athabasca Oil Sands Area
11. AF 2.2.1 Life Cycles of Some Common Aquatic Insects of the Athabasca River, Alberta
12. ME 1.7 Very High Resolution Meteorological Satellite Study of Oil Sands Weather: "A Feasibility Study"
13. ME 2.3.1 Plume Dispersion Measurements from an Oil Sands Extraction Plant, March 1976
- 14.
15. ME 3.4 A Climatology of Low Level Air Trajectories in the Alberta Oil Sands Area
16. ME 1.6 The Feasibility of a Weather Radar near Fort McMurray, Alberta
17. AF 2.1.1 A Survey of Baseline Levels of Contaminants in Aquatic Biota of the AOSERP Study Area
18. HY 1.1 Interim Compilation of Stream Gauging Data to December 1976 for the Alberta Oil Sands Environmental Research Program
19. ME 4.1 Calculations of Annual Averaged Sulphur Dioxide Concentrations at Ground Level in the AOSERP Study Area
20. HY 3.1.1 Characterization of Organic Constituents in Waters and Wastewaters of the Athabasca Oil Sands Mining Area
21. AOSERP Second Annual Report, 1976-77
22. Alberta Oil Sands Environmental Research Program Interim Report to 1978 covering the period April 1975 to November 1978
23. AF 1.1.2 Acute Lethality of Mine Depressurization Water on Trout Perch and Rainbow Trout
24. ME 1.5.2 Air System Winter Field Study in the AOSERP Study Area, February 1977.
25. ME 3.5.1 Review of Pollutant Transformation Processes Relevant to the Alberta Oil Sands Area

26. AF 4.5.1 Interim Report on an Intensive Study of the Fish Fauna of the Muskeg River Watershed of Northeastern Alberta
27. ME 1.5.1 Meteorology and Air Quality Winter Field Study in the AOSERP Study Area, March 1976
28. VE 2.1 Interim Report on a Soils Inventory in the Athabasca Oil Sands Area
29. ME 2.2 An Inventory System for Atmospheric Emissions in the AOSERP Study Area
30. ME 2.1 Ambient Air Quality in the AOSERP Study Area, 1977
31. VE 2.3 Ecological Habitat Mapping of the AOSERP Study Area: Phase I
32. AOSERP Third Annual Report, 1977-78
33. TF 1.2 Relationships Between Habitats, Forages, and Carrying Capacity of Moose Range in northern Alberta. Part I: Moose Preferences for Habitat Strata and Forages.
34. HY 2.4 Heavy Metals in Bottom Sediments of the Mainstem Athabasca River System in the AOSERP Study Area
35. AF 4.9.1 The Effects of Sedimentation on the Aquatic Biota
36. AF 4.8.1 Fall Fisheries Investigations in the Athabasca and Clearwater Rivers Upstream of Fort McMurray: Volume I
37. HE 2.2.2 Community Studies: Fort McMurray, Anzac, Fort MacKay
38. VE 7.1.1 Techniques for the Control of Small Mammals: A Review
39. ME 1.0 The Climatology of the Alberta Oil Sands Environmental Research Program Study Area
40. WS 3.3 Mixing Characteristics of the Athabasca River below Fort McMurray - Winter Conditions
41. AF 3.5.1 Acute and Chronic Toxicity of Vanadium to Fish
42. TF 1.1.4 Analysis of Fur Production Records for Registered Traps in the AOSERP Study Area, 1970-75
43. TF 6.1 A Socioeconomic Evaluation of the Recreational Fish and Wildlife Resources in Alberta, with Particular Reference to the AOSERP Study Area. Volume I: Summary and Conclusions
44. VE 3.1 Interim Report on Symptomology and Threshold Levels of Air Pollutant Injury to Vegetation, 1975 to 1978
45. VE 3.3 Interim Report on Physiology and Mechanisms of Air-Borne Pollutant Injury to Vegetation, 1975 to 1978
46. VE 3.4 Interim Report on Ecological Benchmarking and Biomonitoring for Detection of Air-Borne Pollutant Effects on Vegetation and Soils, 1975 to 1978.
47. TF 1.1.1 A Visibility Bias Model for Aerial Surveys for Moose on the AOSERP Study Area
48. HG 1.1 Interim Report on a Hydrogeological Investigation of the Muskeg River Basin, Alberta
49. WS 1.3.3 The Ecology of Macrobenthic Invertebrate Communities in Hartley Creek, Northeastern Alberta
50. ME 3.6 Literature Review on Pollution Deposition Processes
51. HY 1.3 Interim Compilation of 1976 Suspended Sediment Data in the AOSERP Study Area
52. ME 2.3.2 Plume Dispersion Measurements from an Oil Sands Extraction Plant, June 1977

53. HY 3.1.2 Baseline States of Organic Constituents in the Athabasca River System Upstream of Fort McMurray
54. WS 2.3 A Preliminary Study of Chemical and Microbial Characteristics of the Athabasca River in the Athabasca Oil Sands Area of Northeastern Alberta
55. HY 2.6 Microbial Populations in the Athabasca River
56. AF 3.2.1 The Acute Toxicity of Saline Groundwater and of Vanadium to Fish and Aquatic Invertebrates
57. LS 2.3.1 Ecological Habitat Mapping of the AOSERP Study Area (Supplement): Phase I
58. AF 2.0.2 Interim Report on Ecological Studies on the Lower Trophic Levels of Muskeg Rivers Within the Alberta Oil Sands Environmental Research Program Study Area
59. TF 3.1 Semi-Aquatic Mammals: Annotated Bibliography
60. WS 1.1.1 Synthesis of Surface Water Hydrology
61. AF 4.5.2 An Intensive Study of the Fish Fauna of the Steepbank River Watershed of Northeastern Alberta
62. TF 5.1 Amphibians and Reptiles in the AOSERP Study Area
63. Calculate Sigma Data for the Alberta Oil Sands Environmental Research Program Study Area.
64. LS 21.6.1 A Review of the Baseline Data Relevant to the Impacts of Oil Sands Development on Large Mammals in the AOSERP Study Area
65. LS 21.6.2 A Review of the Baseline Data Relevant to the Impacts of Oil Sands Development on Black Bears in the AOSERP Study Area
66. AS 4.3.2 An Assessment of the Models LIRAQ and ADPIC for Application to the Athabasca Oil Sands Area
67. WS 1.3.2 Aquatic Biological Investigations of the Muskeg River Watershed
68. AS 1.5.3 Air System Summer Field Study in the AOSERP Study Area, June 1977
69. AS 3.5.2
69. HS 40.1 Native Employment Patterns in Alberta's Athabasca Oil Sands Region
70. LS 28.1.2 An Interim Report on the Insectivorous Animals in the AOSERP Study Area
71. HY 2.2 Lake Acidification Potential in the Alberta Oil Sands Environmental Research Program Study Area
72. LS 7.1.2 The Ecology of Five Major Species of Small Mammals in the AOSERP Study Area: A Review
73. LS 23.2 Distribution, Abundance and Habitat Associations of Beavers, Muskrats, Mink and River Otters in the AOSERP Study Area, Northeastern Alberta
- -- Interim Report to 1978
74. AS 4.5 Air Quality Modelling and User Needs
- 75.

- 76. AF 4.5.1 An Intensive Study of the Fish Fauna of the Muskeg River Watershed of Northeastern Alberta
- 77. HS 20.1 Overview of Local Economic Development in the Athabasca Oil Sands Region Since 1961.
- 78. LS 22.1.1 Habitat Relationships and Management of Terrestrial Birds in Northeastern Alberta.
- 79. AF 3.6.1 The Multiple Toxicity of Vanadium, Nickel, and Phenol to Fish.

These reports are not available upon request. For further information about availability and location of depositories, please contact:

Alberta Oil Sands Environmental Research Program  
15th Floor, Oxbridge Place  
9820 - 106 Street  
Edmonton, Alberta  
T5K 2J6

This material is provided under educational reproduction permissions included in Alberta Environment's Copyright and Disclosure Statement, see terms at <http://www.environment.alberta.ca/copyright.html>. This Statement requires the following identification:

"The source of the materials is Alberta Environment <http://www.environment.gov.ab.ca/>. The use of these materials by the end user is done without any affiliation with or endorsement by the Government of Alberta. Reliance upon the end user's use of these materials is at the risk of the end user.